



2022 H. Bolton Seed Memorial Lecture: Evaluating Liquefaction Effects

Jonathan D. Bray, F.ASCE¹; and Franklin R. Olaya, S.M.ASCE²

Abstract: The potential effects of soil liquefaction at level ground sites should be evaluated through examining soil element responses of the individual soil layers and system responses of the soil deposits they form. The cyclic responses and postliquefaction volumetric strain of uniform clean sand, sandy gravel, nonplastic silty sand, and nonplastic silt at the element level can be captured in a unified manner using relative density or the state parameter. The depositional environment should be characterized because geologic details, such as soil fabric, which can be discerned through detailed logging of high-quality continuous sampling, are important in evaluating liquefaction effects. Effective stress analysis enables soil system responses that govern the effects of liquefaction, including the formation of ejecta, to be investigated. A calibrated cone penetration test (CPT) procedure employing the liquefaction ejecta demand parameter captures key aspects of system response and provides an estimate of ejecta-induced building settlement. A probabilistic CPT-based procedure for estimating post-liquefaction ground settlement is developed using laboratory and field case history databases. Correlations are developed to estimate D_r or ψ_o to enable use of the laboratory-based volumetric strain models. Adjustment factors enable the procedure to capture field observations of postliquefaction ground settlement. The proposed ground settlement procedure is combined with shear and ejecta-induced settlement procedures to estimate liquefaction-induced building settlement. **DOI: 10.1061/JGGEFK.GTENG-11242.** © 2023 American Society of Civil Engineers.

Author keywords: Analysis; Case histories; Cone penetration test (CPT); Ejecta; Laboratory; Liquefaction; Settlement; Volumetric strain.

Introduction

The consequences of triggering soil liquefaction in a soil deposit can be negligible to severe. At the element level, the accumulation of shear strain beyond the volumetric threshold shear strain in a soil layer generates excess pore-water pressure that reduces effective stress (Dobry and Ladd 1980). The stiffness and strength of a soil element can degrade rapidly as its effective stress declines to a low value. Understanding, characterizing, and modeling the cyclic response of a soil unit that is susceptible to liquefaction are crucial to evaluating the effects of liquefaction at a site. However, the system response of the entire soil deposit should also be evaluated to assess the effects of soil liquefaction at the site. For example, a site with a nearby free-face slope that imposes a significant static driving stress can undergo a damaging lateral spread if a continuous soil layer liquefies. Conversely, gently sloping ground with isolated soil units that liquefy may not displace because the liquefied soil units are not laterally continuous. At some level ground sites, the formation of sediment ejecta produces extensive ground cracking and the loss of foundation support, which damages infrastructure. At other level ground sites, earthquake shaking triggers soil liquefaction in a deep soil layer that is well below building foundations, so that

Note. This manuscript was submitted on August 5, 2022; approved on April 19, 2023; published online on June 6, 2023. Discussion period open until November 6, 2023; separate discussions must be submitted for individual papers. This paper is part of the *Journal of Geotechnical and Geoenvironmental Engineering*, © ASCE, ISSN 1090-0241.

damaging shear-induced displacement does not develop. In these cases, the dissipation of the excess pore-water pressure in the soil can still produce ground settlement due to sedimentation and reconsolidation volumetric strain processes; however, the ground settlement may be uniform and moderate, so it causes no infrastructure damage.

Performance-based engineering requires robust methods to evaluate liquefaction effects. Nonlinear dynamic soil structure interaction (SSI) effective stress analyses can provide key insights as well as reasonable estimates of liquefaction-induced ground and building movements. Nonlinear effective stress analysis can capture the element response of soil and the system response of the soil deposit, if performed with sound soil constitutive models that are calibrated and validated to capture the element response of soil and employed in numerical models that capture system response features (e.g., seismic site response, soil layering, and water flow). Alternatively, empirical procedures may be used in engineering practice because they can be calibrated to reliably estimate the observed ground and building performance. Researchers have developed empirical procedures to estimate liquefaction-induced ground settlement and lateral movement using field case history data with models informed by laboratory test results and mechanics. In these methods, the complex processes involved in liquefaction triggering and its consequences are captured using proxies that represent the state of the soil and the seismic demand. For example, cone penetration test (CPT)-based empirical methods for estimating liquefaction-induced level-ground settlement and sloping ground lateral spread displacement methods are widely used in engineering practice (e.g., Zhang et al. 2002, 2004). There is merit to developing alternative methods, especially if the empirical methods are informed by new field case histories that explore the response of a wider range of soil types and seismic demands.

This work explores soil liquefaction effects of level ground sites composed of sand, sandy gravel, silty sand, nonplastic silt, and slightly plastic clayey silt with and without structures. The element

¹Distinguished Professor, Dept. of Civil and Environmental Engineering, Univ. of California, Berkeley, Berkeley, CA 94720-1710 (corresponding author). ORCID: https://orcid.org/0000-0001-9368-4365. Email: jonbray@berkeley.edu

²Ph.D. Graduate Student Researcher, Dept. of Civil and Environmental Engineering, Univ. of California, Berkeley, Berkeley, CA 94720-1710. ORCID: https://orcid.org/0000-0003-1896-912X. Email: folaya@berkeley.edu

and system responses of the individual soil layers and the soil deposits they form are examined. Soil system responses are investigated to characterize the severity of soil ejecta, so its effects on infrastructure can be assessed. A probabilistic CPT-based procedure for estimating postliquefaction ground settlement is presented. Recommendations for its use in engineering practice are shared.

Liquefaction-Induced Building Movements

Liquefaction has the potential to damage buildings. The bearing capacity failure of buildings, such as the five-story building in Adapazari, Turkey, in Fig. 1(a), the settlement and lateral displacement of another building in Adapazari in Fig. 1(b), and the ejecta-induced settlement of a two-story building in Christchurch, New Zealand, in Fig. 1(c) illustrate some of the direct consequences of liquefaction on buildings with shallow foundations (Bray and Stewart 2000; Bray et al. 2004, 2014b). The fire shown in Fig. 1(d) that consumed part of Kobe, Japan, reminds engineers of the indirect consequences of liquefaction that can devastate a city (Akai et al. 1995). In numerous other postearthquake photographs (not shown), there is no discernable damage to buildings even though current procedures indicate the factor of safety against liquefaction triggering (FS_L) is well below one (e.g., Beyzaei et al. 2018a). Thus, the effects of liquefaction on buildings can be negligible to severe.

Several of the key mechanisms of liquefaction-induced building settlement are illustrated in Fig. 2. They can be categorized as shear-induced, volumetric-induced, or ejecta-induced deformation, and estimated separately as recommended by Bray and Macedo (2017). Alternatively, the mechanisms can be combined in estimating liquefaction-induced building settlement as recommended by

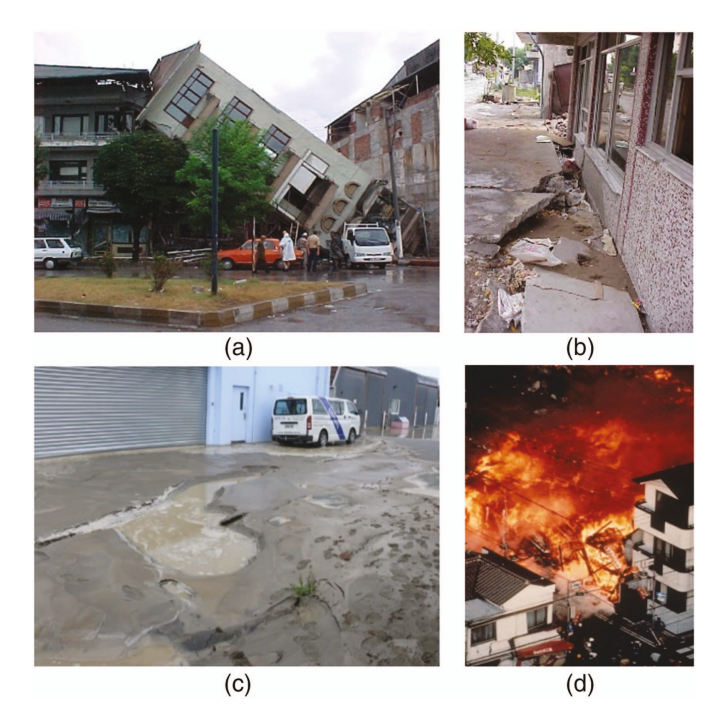


Fig. 1. (Color) Buildings damaged by liquefaction: (a) overturned fivestory building in Adapazari; (b) laterally displaced and settled building in Adapazari; (c) ejecta affecting building in Christchurch; and (d) fire in Kobe. [Images (a, b, and d) courtesy of PEER, University of California, Berkeley; image (c) by Jonathan D. Bray.]

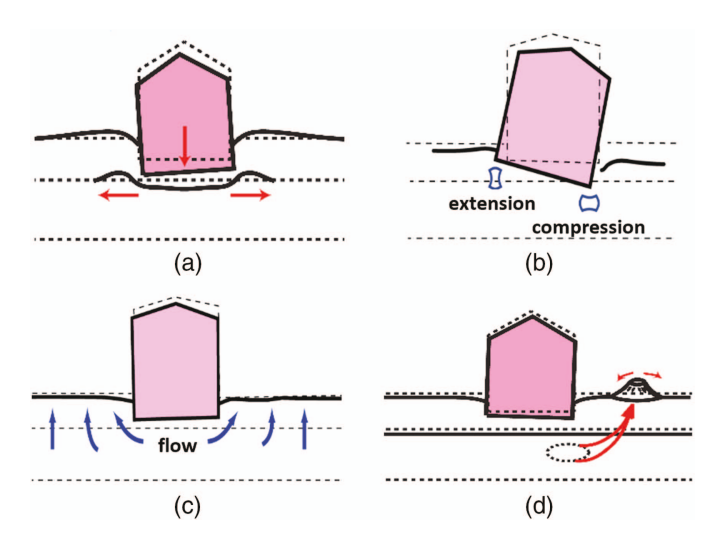


Fig. 2. (Color) Liquefaction-induced building displacement mechanisms: (a) shear-induced punching failure; (b) shear-induced SSI ratcheting; (c) volumetric-induced reconsolidation settlement; and (d) ejecta-induced ground loss.

Bullock et al. (2019). The former approach is employed in this study to examine the contribution of each component of settlement. Ejecta are not produced in some cases (i.e., thick nonliquefiable crust overlying a thin liquefied soil layer) and are severe in other cases, so there is merit to separating this component from the other two mechanisms. Moreover, the shear-induced component of settlement governs in some cases, and in other cases when the liquefiable layer is deep, it is negligible. Lastly, uniform volumetric-induced ground settlement contributes to total building settlement without tilt, whereas differential volumetric-induced ground settlement contributes to differential building settlement and tilt. Bray and Macedo (2017) proposed a CPT-based probabilistic method to estimate shear-induced liquefaction building settlement. Hutabarat and Bray (2022) proposed a CPT-based method to categorize liquefaction ejecta severity, which is used in this work to develop an estimate of this component of settlement. A probabilistic CPTbased method to estimate volumetric-induced ground settlement is proposed. Before discussing these topics, it is useful to summarize some of the key aspects of soil liquefaction at the element and system response levels.

Soil Liquefaction at the Element Level

Clean Uniform Sand

Much of the profession's understanding of soil liquefaction is based on laboratory experiments and field case histories involving clean uniform sand. For example, the Boulanger and Idriss (2016) empirical CPT-based liquefaction triggering procedure is largely based on sites with relatively thick deposits of clean sand or silty sand with fines contents $(FC) \leq 35\%$. Fewer than 14% of their case histories contain critical layers with FC > 35%. Experiments that shape our understanding of liquefaction have been conducted largely on laboratory-prepared specimens of clean sand (e.g., Seed 1979). Silty soils have been tested less frequently (e.g., Bray and Sancio 2006). Even well-graded clean sands have been tested less frequently than uniform clean sand. The reference material for many of our liquefaction assessment methods are clean uniform sand and the state of well-graded sand, silty sand, and silt is

adjusted to reflect that of a uniform clean sand with equivalent cyclic responses [i.e., through a clean sand equivalent penetration resistance, such as the CPT q_{c1ncs} (Boulanger and Idriss 2016)]. There is an implicit assumption, when applying empirically based liquefaction procedures and concepts to a wide range of soils, that they can be adjusted to adequately capture the cyclic response and performance of soils other than clean uniform sand. For example, the response of a silty soil with initially a low q_{c1n} value can be grouped with a clean sand that has a higher q_{c1n} value if the silty sand's "corrected" penetration resistance q_{c1ncs} equals the q_{c1n} of the clean sand. Research investigating the validity of this assumption in the evaluation of the effects of liquefaction is limited, which contributes to uncertainty in applying uniform clean sand methods to other soil types (Bray et al. 2017).

Relative Density and State Parameter

Relative density (D_r) is used along with effective confining stress to characterize the state of clean sand. Cubrinovski and Ishihara (2002) found the Japanese Standard JIS A 1224:2009 (JGS 2000) Test Method yielded consistent maximum void ratio (e_{max}) and minimum void ratio (e_{\min}) values for silty sand with nonplastic FC up to 35% for a comprehensive database with over 300 native soils. Reexamination of their database found that reasonable $e_{
m max}$ and e_{\min} values were also obtained for nonplastic soils with even higher FC (Mijic et al. 2021a). Additionally, Mijic et al. (2021a) obtained repeatable $e_{\rm max}$ and $e_{\rm min}$ values for Christchurch relatively uniform nonplastic silty sand and sandy silt with $FC \le 70\%$; and the dispersion in the $e_{
m max}$ and $e_{
m min}$ values of nonplastic silt with FC = 100% was small. Tests on a wide range of uniform nonplastic soil indicate that, initially, $e_{\rm max}$ decreases slightly with increasing FC from 0% to about 30%, and then increases with a higher rate of increase with increasing FC > 30%; and e_{\min} tends to decrease with increasing FC from 0% to about 30%-40% and increases slightly from approximately 40%-100% fines (e.g., Cubrinovski and Ishihara 2002; Thevanayagam et al. 2002; Mijic et al. 2021a). Thus, $FC \approx 30\%$ is the approximate threshold for a finesdominated particle structure for many silty sands. With e_{max} and e_{\min} measured in a consistent manner, the responses of uniformly graded nonplastic sand, silty sand, and silt at the same D_r can be

Soil can also be characterized with the initial state parameter (ψ_a) defined as

$$\psi_o = (e_o - e_c)|_{p_o'} \tag{1}$$

where e_o = current void ratio at its current mean effective stress (p'_o) ; and e_c = void ratio at the critical state at the same p'_o (Been and Jefferies 1985). The initial state parameter is useful to describe the response of many soil types over a wide range of stress levels and loading conditions. It captures the key influences of soil density and effective confining stress, as well as other factors such as soil compressibility, grain size, and grain shape, and thus is more informative than D_r . Jefferies and Been (2016) found $\psi_o = -0.05$ to be the threshold between contractive and dilative volumetric responses in simple shear tests. Slightly more negative values of $\psi_o = -0.08$ were observed in isotropic triaxial compression tests. Considering field stress conditions, partial drainage, and field case histories characterized by the CPT, they concluded that $\psi_o = -0.05$ was a reasonably conservative threshold to use in practice. Shuttle and Cunning (2007, 2008) identified from large-scale flow slide case histories that $\psi_o = -0.05$ is a reasonable threshold between contractive and dilative response tendencies, and Robertson (2016) and Mayne and Styler (2018) also use $\psi_o = -0.05$ as a suitable threshold of contractive or dilative responses in the field. This slightly negative value of the initial state parameter is consistent with the lower position of the quasi-steady-state line (QSSL) relative to the steady-state line (SSL). The QSSL captures the fabric-dependent phase transformation response of soil that affects its liquefaction triggering resistance and QSS shear strength. Thus, $\psi_o=-0.05$ is a practical threshold to discern contractive versus dilative responses in the field.

Nonplastic Silty Soil Liquefaction

Polito and Martin (2001), Bray and Sancio (2006), Beyzaei et al. (2018a), Markham et al. (2018), Mijic et al. (2021b), and other researchers have shown that nonplastic silty soils liquefy in a manner like many clean sands. They often exhibit a cyclic mobility response due in part to the angularity of many silt-size particles. As an example, the representative responses of three cyclic simple shear (CSS) 16-mm-thick test specimens composed of relatively homogeneous high-quality samples of different natural soil units in Christchurch are shown in Fig. 3 (Mijic et al. 2021b). The Unified Soil Classification System (USCS) classifications for these soils are uniform sand (SP) with FC = 2%, silty sand (SM) with nonplastic FC = 44%, and silt (ML) with nonplastic FC = 64%, with their grain size distributions shown in Fig. 4(a) and their particle shapes shown in Fig. 4(b). These soils are of uniform gradation and composed of angular particles. The SP, SM, and ML test specimens have similar D_r values of 88%, 80%, and 82%, and similar ψ_o values of -0.13, -0.11, and -0.07, respectively, based on their SSLs, and they were tested with similar cyclic stress ratios (CSR) of 0.16 to 0.22. Their cyclic responses are similar in terms of shear stress versus shear strain and the development of excess pore-water

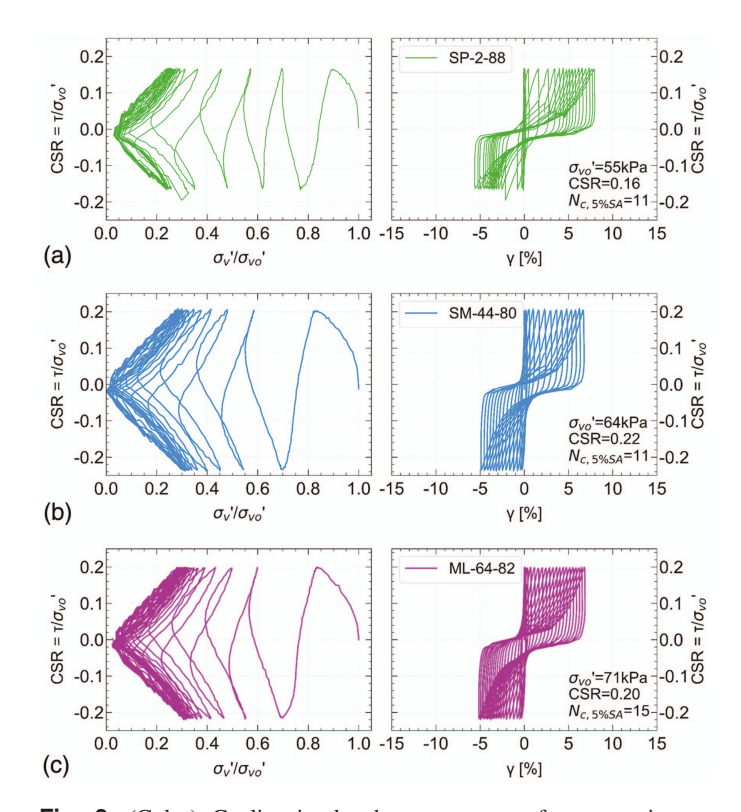


Fig. 3. (Color) Cyclic simple shear response of test specimens: (a) SP-2-88; (b) SM-44-80; and (c) ML-64-82, where the Unified Soil Classification System designation is USCS-FC- D_r . (Data from Mijic et al. 2021b.)

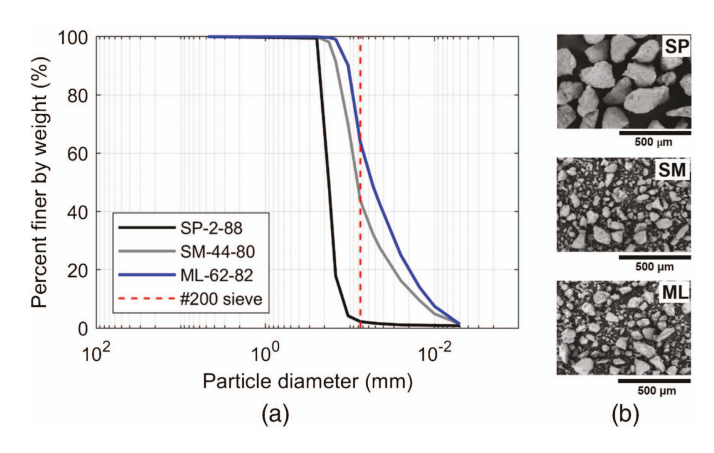


Fig. 4. (Color) (a) Grain size distributions of sand, silty sand, and silt tested in southwest Christchurch with (b) SEM images of the soil particles. (Data from Mijic et al. 2021b.)

pressure as indicated by the changes in the normalized vertical effective stress (σ'_v/σ'_{vo}) .

The finer fraction of a nonplastic silty sand controls particle fabric and the response of soils with FC greater than about 30% (Cubrinovski and Ishihara 2002; Thevanayagam et al. 2002). Therefore, a nonplastic silty sand with FC > 30% should respond like a nonplastic silt, which is confirmed by the comparison of the SM and ML material responses shown in Figs. 3(b and c). Moreover, the cyclic response of a uniform fine sand should not differ appreciably from that of a uniform coarse nonplastic silt if their mineralogy, particle shape, etc., are the same; and, by inference, it should not differ appreciably from a nonplastic uniform silty sand. Fines content does not discriminate the mechanical responses of uniform soils of the same mineralogy and particle shape for these cases because little fundamentally changes as a uniform grain size distribution is shifted horizontally across the #200 sieve threshold. A particle size threshold of 0.075 mm does not separate fundamentally different soil responses to monotonic or cyclic loading. Mineralogy, particle shape, etc., are more important in determining the cyclic responses of uniform fine sand and uniform coarse silt.

Conversely, Cubrinovski and Ishihara (2002) and Jefferies and Been (2016) showed that, with all other conditions maintained, nonplastic fines increased a sand's compressibility, which reduces its penetration resistance significantly and reduces its cyclic resistance ratio (CRR). However, the soils they investigated were often well-graded. Fines content is informative for well-graded soils. Changes in the tail of the grain size distribution curve reflect changes in soil compressibility which, in turn, affects CRR, although fines content affects penetration resistance more than CRR.

Clayey Silt Liquefaction

Extensive liquefaction of clayey silt in Adapazari during the 1999 Kocaeli earthquake led to research that developed the Bray and Sancio (2006) plasticity index (PI) ≤ 12 and water content-to-liquid limit ratio (w/LL) ≥ 0.85 criteria for the liquefaction susceptibility of fine-grained soil. Their initial hypothesis was that liquefaction susceptibility would decline systematically as PI increased, but they could not discern significant changes in the cyclic responses of the natural clayey silt soils in the results of over 100 cyclic triaxial tests of high-quality samples of natural soils. Their PI ≤ 12 criterion is similar to the finding of Ishihara (1993) that fine-grained soils with PI ≤ 10 do not differ in their CRR, whereas CRR increases systematically as PI increases in soils

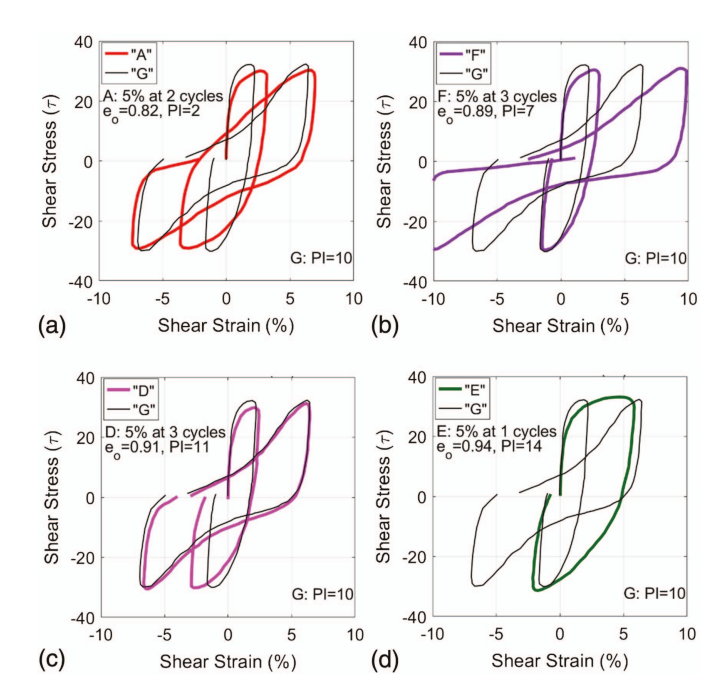


Fig. 5. (Color) Cyclic simple shear test results of Adapazari silt of various PIs: (a) PI = 2; (b) PI = 7; (c) PI = 11; and (d) PI = 14. First cycle and cycle to reach 5% shear strain are compared to Soil "G" with PI = 10 ($e_o = 0.68$). Soil "G" reaches 5% shear strain at 7 cycles. All tests have $\sigma_v' \approx 137$ kPa and CSR ≈ 0.21 (data from Donahue et al. 2007).

with PI > 10. The Idriss and Boulanger (2008) PI < 7 liquefaction susceptibility criterion is sometimes compared with the Bray and Sancio PI ≤ 12 criterion, but comparison of these criteria should consider their different definitions of liquefaction. In the use of their criterion, Idriss and Boulanger (2008) reserve the term liquefaction to soils that can be evaluated using penetration resistance (e.g., CPT tip resistance); whereas Bray and Sancio (2006) use the term liquefaction for fine-grained soils if their stress–strain responses in cyclic tests are like the stress–strain response of clean sand that are classified as liquefiable. Bray and Sancio (2008) and Boulanger and Idriss (2008) agree that clayey silt soil can be sampled effectively, and therefore, laboratory testing should be used to characterize the cyclic response of these soils so that the consequences of their responses can be evaluated.

Although the Bray and Sancio (2006) test specimens used to develop their liquefaction susceptibility criteria were relatively homogeneous, they possessed some variability as natural soil deposits. Donahue et al. (2007) prepared more homogeneous CSS test specimens by reconstituting them from mixtures of Adapazari silt and clay to explore this issue further. Representative test results of the first load cycle and load cycle to reach 5% shear strain are shown in Fig. 5. The cyclic responses of the test specimens with PI = 2, 7, 10, and 11 are similar, and hence, should be considered similarly in terms of their cyclic responses in performance-based engineering assessments. The PI = 14 test specimen displays "claylike" behavior that differs noticeably from the lower PI test specimens shown in Fig. 5. In another study, Beyzaei et al. (2018a) tested several Christchurch soils that included clean sand, nonplastic silt, and PI = 10 silts, whose test results are shown in Fig. 6. The cyclic responses of the uniform fine clean sand and the PI = 10silt test specimens are nearly identical, with the nonplastic silt deviating only slightly from their responses, although in part because a higher CSR was applied to it. Thus, it is prudent to characterize

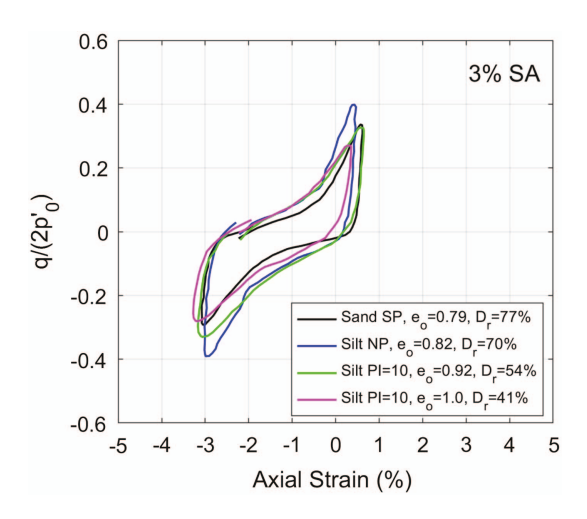


Fig. 6. (Color) Stress–strain response for 3% single-amplitude (SA) axial strain; specimens reach 3% SA at 5 cycles, 4 cycles, 5 cycles, and 9 cycles for sand (EQC4-DM1B-7U-A), nonplastic silt (S21-DM1-3U-A), PI = 10 silt (S33-DM1-8U-A), and PI = 10 silt (S33-DM1-8U-B), respectively. (Data from Beyzaei et al. 2020.)

the cyclic response of clayey silts (whether eventually termed liquefaction or cyclic failure) through a program of laboratory testing that includes consolidation tests, monotonic tests, and cyclic tests performed on high-quality retrieved natural soil test specimens.

System Response of Soil Deposits Containing Liquefiable Soils

System Response Factors

Although soil composed of angular nonplastic silt particles or low-plasticity clayey silt can liquefy in terms of developing high excess pore-water pressure and shear strain, the effects of liquefaction can differ greatly from those of loose clean sand. For example, the vertical hydraulic conductivity (k_v) of a soil unit plays an integral role in movement of water during and after earthquake shaking. The fine sand, nonplastic silty sand, nonplastic silt, and plastic silt tested by Beyzaei et al. (2018a) have $k_v \approx 10^{-2}$ cm/s, 10^{-3} cm/s, 10^{-4} - 10^{-5} cm/s, and $<10^{-6}$ cm/s, respectively. The wide range of hydraulic conductivities of these soil units in stratified soil deposits will greatly affect the vertical flow of water in the soil deposit and, hence, its system response.

Several researchers have explored various aspects of the system response of soil deposits during earthquake shaking. Cubrinovski et al. (2018b) identified several key factors affecting the development and consequences of liquefaction. The manifestation of liquefaction at the surface of free-field level ground sites depends primarily on the thickness and vertical continuity of critical layers and other liquefiable materials in the deposit. Sites with thick zones of liquefiable soils in the top 10 m tend to produce ejecta, and interbedded deposits of liquefiable and nonliquefiable soil layers do not.

Fig. 7 illustrates the important role of soil deposit stratification in the formation of ejecta. CPT profiles of tip resistance (q_c) and soil behavior type index (I_c) at free-field Christchurch sites that produced ejecta are shown with red traces and sites without ejecta are shown with blue traces (Beyzaei et al. 2018b). The influence of peak ground acceleration (PGA) is shown by binning the CPT profiles by median estimated PGA_{M6} scaled to moment magnitude

 $(M_w) = 6.0$ (Beyzaei et al. 2018b). When $0.2 g < PGA_{M6} < 0.4 g$, sites with ejecta had thick layers of clean sand with I_c consistently less than 1.8, whereas sites without ejecta had highly stratified silt/ sand deposits as indicated by highly variable I_c profiles. Many of the stratified soil sites shown in Fig. 7 without surface manifestations of liquefaction (i.e., no ejecta) are cases in which liquefactiontriggering procedures indicate that liquefaction should have occurred. Cyclic triaxial (CTX) tests indicate that many of the soil units at these sites liquefied at the element level at these ground motion intensity levels (Beyzaei et al. 2018a). However, they did not produce ejecta because low hydraulic conductivity silty soil layers resisted the vertical movement of water up through the soil profile. When $PGA_{M6} > 0.4 g$, more stratified silt/sand deposits produced ejecta, indicating the likelihood of ejecta increases for stratified soil sites at intense shaking levels. Sites with heavy buildings can also produce ejecta at lower levels of shaking due to SSI effects (Bray et al. 2004; Bray and Macedo 2017).

Effective stress analysis of thick clean sand deposits and stratified silty soil deposits by Hutabarat and Bray (2021a, b) confirm that the postshaking hydraulic characteristics of the soil profiles (i.e., soil layer stratification, vertical hydraulic conductivity profile, and depth of liquefaction triggering) largely determine if ejecta will or will not be produced if strongly shaken. Representative thick clean sand and stratified silty soil deposits in Christchurch are shown in Fig. 8. The modified soil behavior type index (I_R) (Robertson 2016) shown in Fig. 8 is useful in calibrating effective stress soil constitutive models to capture the sandlike or claylike responses and contractive or dilative responses of soil units. The Ti Rakau site [Fig. 8(a)] has a thick deposit of liquefiable clean sandlike material (i.e., $I_B > 32$) beneath a nonliquefiable crust. Parts of the thick clean sand unit liquefied, and other parts of it generated high excess pore-water pressures during the 2011 Christchurch and June earthquakes and produced severe ejecta (Hutabarat and Bray 2021b). As shown in Fig. 9(a), liquefaction of a high k_v sand unit produces excess hydraulic head (h_e) that generates upward water flow. Its high excess pore-water pressure is sustained by upward seepage from deeper hydraulically connected high k_v sand units that also generate significant excess pore-water pressure. Assuming the groundwater level rises to the ground surface in cracks formed in the crust layer, the excess hydraulic head required to generate a hydraulic gradient sufficient to produce significant ejecta is assumed to be represented by a 1H:1V line on the h_e versus depth profile shown in Fig. 9(b). The 1H:1V line is adopted as the critical threshold of excess hydraulic head required to initiate and to manifest significant ejecta at the ground surface, which is termed the critical excess hydraulic head (h_c) . Conversely, the highly stratified Gainsborough site [Fig. 8(b)] produced no ejecta during the Canterbury earthquakes, even though it was shaken intensely by the 2010 Darfield, 2011 Christchurch, and 2011 June earthquakes. Effective stress analyses calibrated by established field and laboratory test methods indicate that some soil layers at the Gainsborough site liquefied and other layers developed significant excess pore-water pressure, but they were relatively thin and isolated. High excess pore-water pressures did not develop over a thick zone directly beneath the nonliquefiable crust, and h_e never exceeded that required to manifest ejecta (h_c) .

Effective stress analysis can reveal key system response characteristics that dictate the effects of liquefaction at a site (e.g., Cubrinovski et al. 2018b; Hutabarat and Bray 2021a, b). The occurrence of sediment ejecta and its severity depend significantly on hydraulic processes after strong ground shaking ceases, which the simplified liquefaction triggering procedures do not consider. The excess hydraulic head calculated in effective stress analysis captures the seismically induced hydraulic demand generated by earthquake shaking

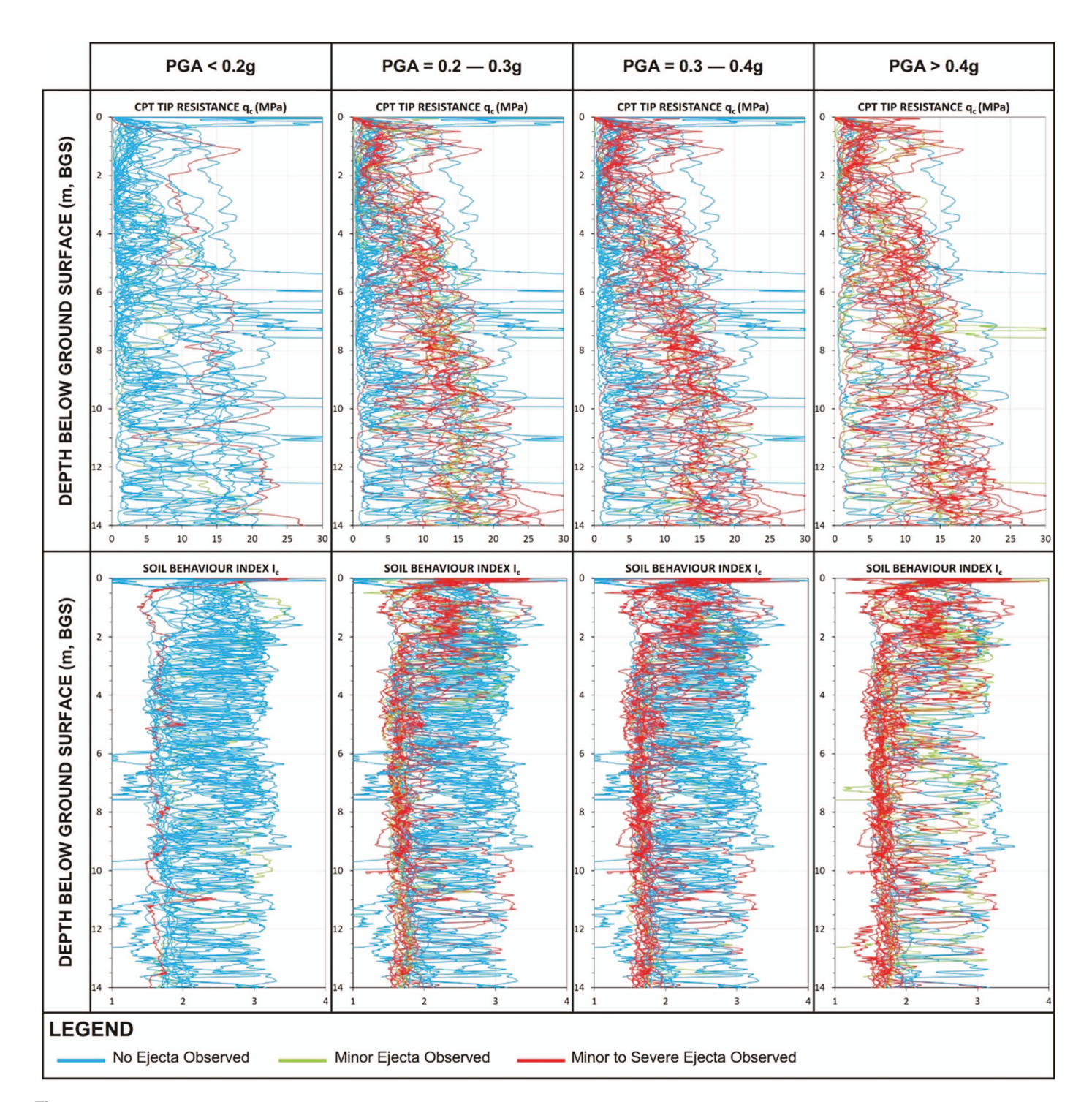


Fig. 7. (Color) CPT tip resistance (q_c) and soil behavior type index (I_c) profiles for selected sites throughout Christchurch. Liquefaction observations are shown in: blue (no ejecta within 50-m radius of CPT), green (minor ejecta: <5% of ground surface covered by ejecta within 50-m radius of CPT), and red (minor to severe ejecta: >5% of ground surface covered by ejecta within 50-m radius of CPT) for the four main events of the Canterbury earthquake sequence for median PGA shaking levels for an equivalent M_w 6.0 event. (Data from Beyzaei et al. 2018a.)

and its evolution after shaking. The integration of the excess hydraulic head exceeding the 1H:1V line [illustrated by the shaded area shown in Fig. 9(b)] with time over a period of 180 s after the start of ground shaking produces the ejecta potential index (EPI). Hutabarat and Bray (2021b) showed that EPI captures the advection processes that govern the amount of upward seepage-induced flow that determines ejecta severity. Sites with severe ejecta have high EPI values, and sites without ejecta have low EPI values. Although effective stress analysis of the seismic response of a liquefiable site provides

great insight, it may be infeasible to perform advanced analysis for projects with limited subsurface data and ground motion recordings. Thus, the development of a reliable CPT-based procedure that does not require effective stress analysis has merit.

CPT-Based Ejecta Severity Procedure

The Hutabarat and Bray (2022) CPT-based liquefaction ejecta assessment procedure employs two governing parameters: liquefaction

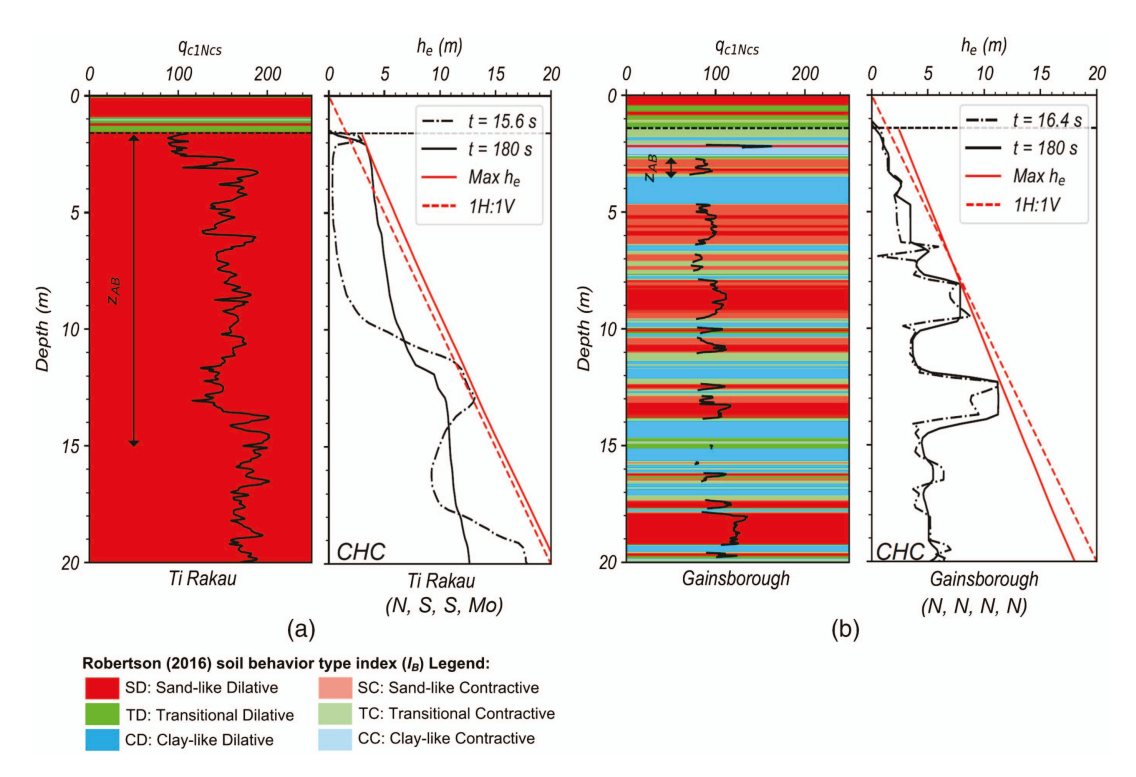


Fig. 8. (Color) (a) Representative thick sand; and (b) stratified soil site profiles of q_{c1Ncs} , I_B , and observed ejecta severity (given below site name in the sequence of the DAR, CHC, JUN, and DEC earthquakes where N = None; Mi = Minor; Mo = Moderate; S = Severe; and E = Extreme).

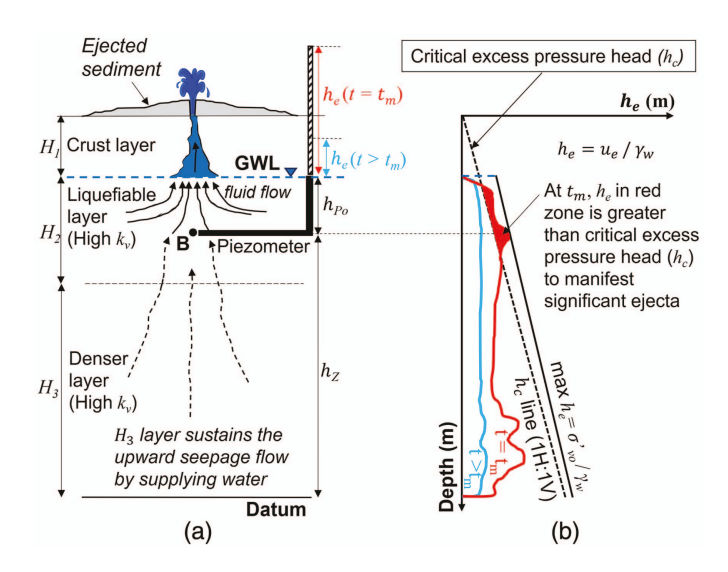


Fig. 9. (Color) (a) Sediment ejecta mechanisms in a typical thick sand site; and (b) ejecta potential index concept.

ejecta demand (L_D) and crust layer resistance (C_R) . The L_D parameter considers the excess hydraulic head (h_e) that can produce upward water flow sufficient to manifest ejecta, and the C_R parameter considers the thickness of the nonliquefiable crust layer and its equivalent shear strength that suppresses manifestations of liquefaction. L_D is estimated as follows:

$$L_D \text{ (kN/m)} = \gamma_w \int_{z_A}^{z_B} \frac{k_v}{k_{cs}} (h_e - h_c) dz \begin{cases} \text{when } h_e \ge h_c \\ 0, \text{ otherwise} \end{cases} \tag{2}$$

where z_A = depth from the ground surface to the top of the shallowest soil layer below the groundwater level with I_c < 2.6 that is at least

250-mm-thick; z_B = depth from the ground surface to the top of the shallowest soil layer between the depths of z_A and 15 m with $I_c \ge 2.6$ that is at least 250-mm-thick; and k_{cs} = baseline vertical hydraulic conductivity of clean sand with $I_c = 1.8$ [with k_v estimated using the Robertson and Cabal (2015) correlation]. A soil layer's k_v directly influences the upward flow of water in a soil column that can induce postshaking secondary liquefaction at shallow depths, which generates ejecta. The water flowing upward from a deep liquefied layer can increase the h_e in a shallow layer if the intermediate soil layers have high k_v values. Conversely, a low- k_v intermediate-depth soil layer with sufficient thickness can restrict the upward flow of water from deep liquefiable layers. To capture this effect, the normalized- k_v weighting factor (k_v/k_{cs}) is employed, so a low-permeability layer decreases L_D and a high-permeability layer increases L_D . The parameter z_{AB} (defined as the thickness of the first continuous sandlike soil layer that liquefies beneath the nonliquefiable crust) is also an indicator of the potential to generate sufficient upward seepage to produce ejecta. In the comparison of the two sites shown in Fig. 8, the parameter z_{AB} at the Ti Rakau site [Fig. 8(a)] that produced severe ejecta is over 13-m-thick, whereas it is less than 1-m-thick at the Gainsborough site [Fig. 8(b)] that did not produce

The other parameter C_R is estimated as

$$C_R \text{ (kN/m)} = \int_{0m}^{H_1} s_u dz \begin{cases} s_u = K_o \sigma'_{vo} \tan(\phi_{cs}), & \text{if } I_B > 22\\ s_u = \frac{(q_t - \sigma_{vo})}{N_{kt}}, & \text{if } I_B \le 22 \end{cases}$$
(3)

where H_1 (m) = thickness of the layer above z_A until the ground surface; s_u (kN/m²) = shear strength of the crust layers estimated using CPT data; K_o = coefficient of lateral earth pressure, which is assumed to be 0.5; ϕ_{cs} = critical state friction angle, which is

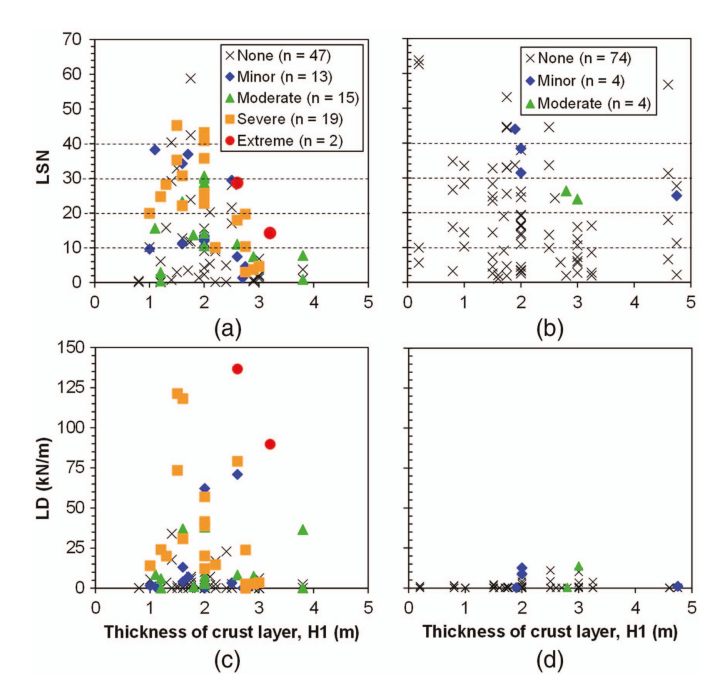


Fig. 10. (Color) Distribution of liquefaction ejecta demand parameters versus crust thickness for field case histories from Hutabarat and Bray (2022).

assumed to be 33°; and $N_{kt} = 15$ in the tip resistance (q_t) correlation used for clay. A clay-like soil with $I_B \le 22$ will have a higher s_u than a crust layer composed of sand-like or transitional soil defined by $I_B > 22$, because the vertical effective stress is low at shallow depths. Thus, s_u represents the strength (and integrity) of the crust.

The liquefaction ejecta demand parameter captures the effects of system response mechanisms that the simplified liquefaction triggering procedure was never intended to capture. L_D also performs better than other liquefaction indices, such as liquefaction potential index (LPI) (Iwasaki et al. 1978) and liquefaction severity number (LSN) (van Ballegooy et al. 2014), because L_D applies the normalized- k_v as a weighting factor to the estimated h_e at each depth in the soil profile. The performance of L_D is compared with the performance of LSN at thick clean sand sites and stratified silty soil sites in Christchurch in Fig. 10 (Hutabarat and Bray 2022). Simplified liquefaction triggering procedures, LPI, and LSN overestimate the manifestation of liquefaction at stratified soil sites [e.g., LSN varies from 2 to 65 at sites that had no ejecta, Fig. 10(b)]. L_D resolves the overestimation tendency of the other liquefaction indices, as its values are low (i.e., L_D < 5 except for two cases with L_D = 10) for 74 stratified silty soil sites that had no ejecta [Fig. 10(d)]. Additionally, L_D tends to be low at thick clean sand sites that had no ejecta, and tends to be high for thick clean sites with severe and extreme ejecta severity. LSN also performs reasonably well at thick clean sand sites [Fig. 10(a)]; however, close examination of Figs. 10(a and c) indicate that L_D performs slightly better than LSN at these sites.

Combining the crust layer resistance parameter with the lique-faction ejecta demand parameter—both of which can be calculated using CPT data—improves the performance of the liquefaction-induced ejecta severity estimation, because ejecta severity diminishes as the nonliquefiable crust layer becomes more resistant to ejecta formation. The resulting Hutabarat and Bray (2022) $L_D - C_R$ chart shown in Fig. 11 estimates the severity of ejecta at free-field level ground sites. The $L_D - C_R$ chart generally estimates ejecta severity well for the 176 case histories investigated by Hutabarat

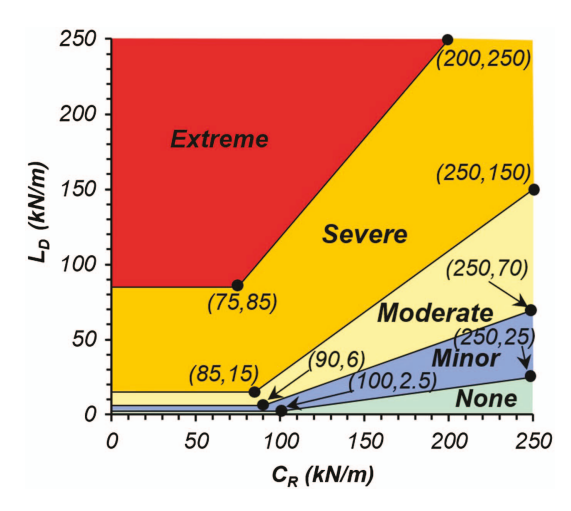


Fig. 11. (Color) Liquefaction-induced ejecta severity chart defined by liquefaction demand (L_D) and crust resistance (C_R) parameters. (Reprinted from Hutabarat and Bray 2022, © ASCE.)

and Bray (2022). Ejecta severity was categorized by the percentage of the total area within 20 m of the site covered by ejecta as described in Table 1. The true positive rate (TPR) calculated as TPR = TP/(TP + FN), where TP = number of true positive cases and FN = number of false negative cases, provides a quantitative measure of the efficacy of the $L_D - C_R$ chart and other liquefaction indices. TPR is 88% for the L_D-C_R chart and 18% for LSN for the 74 cases that produced no ejecta in the Canterbury earthquakes (Hutabarat and Bray 2022). Thus, the $L_D - C_R$ chart resolves the overestimation problem of the other indices at highly stratified soil sites. The improvement is largely because L_D captures the important role of low- k_n layers by impeding upward seepage, which prevents ejecta production at stratified soil sites. TPR is 66%, 15%, 27%, and 74% for the $L_D - C_R$ chart and 49%, 46%, 20%, and 21% for LSN for thick clean sites with no ejecta (47 cases), minor ejecta (13 cases), moderate ejecta (15 cases), and severe ejecta (19 cases), respectively. Thus, in three of the four ejecta severity categories, the $L_D - C_R$ chart performs better than LSN at thick clean sites, and for two of these categories, the difference in the TPR values is significant.

Ejecta-Induced Ground Settlement

The field case history observations available to classify ejecta severity have generally been in the form of the percentage of an area of ground covered by ejecta. Ejecta coverage at a site is an indicator of ejecta-induced ground settlement. However, there are other factors to consider, such as conditions that can produce a large volume of ejecta within a small area, for example, due to a defect in the crust (i.e., utility pole) or the presence of a discontinuous water barrier (i.e., the edge of a reinforced concrete slab-on-grade foundation). Sites with localized ejecta produce more ejecta-induced settlement in these areas than sites with ejecta distributed over a broad area. Tonkin & Taylor estimated localized and distributed ejecta-induced settlement and the percentage of area of ground covered by ejecta at many Christchurch sites using LiDAR surveys and field observations (S. van Ballegooy et al. personal communication, 2018). They related the localized and distributed ejecta-induced ground settlement measurements to the previously mentioned ejecta severity categories based on the area covered by ejecta as shown in Table 1. The ejecta-induced settlement estimates based on the area covered by ejecta are approximate. However, this approach enables

Table 1. Ejecta severity and settlement from field surveys

Ejecta severity category ^a	Area within 20 m covered by ejecta (%)	Estimated localized ejecta-induced settlement (mm)	Estimated distributed ejecta-induced settlement (mm)
None	0	0	0
Minor	<5	0-50	0-20
Moderate	5-20	0-100	10-50
Severe	20-50	50-300	25-150
Extreme	>50	200-500	100-300

Source: Data from S. van Ballegooy, personal communication, 2018. ^aEjecta severity category is determined by the area within 20 m covered by ejecta.

an engineer to judge when localized building settlement due to the ejecta mechanism will likely be 0 (None category), ≤50 mm (Minor category), ≤100 mm (Moderate category), or larger (Severe-Extreme categories).

The recent development of the Mijic et al. (2022) ejecta-induced settlement database provides an alternative approach. Mijic et al. (2022) developed 225 case histories that document the occurrence and quantity of ejecta for 61 free-field level ground sites affected by the 2010–2011 Canterbury earthquake sequence. Photographic evidence and aerial LiDAR measurements were used to estimate the amount of ejecta produced at the sites for the four primary Canterbury earthquakes. Areal ejecta-induced ground settlement was estimated over the entire selected assessment area, whereas localized ejecta-induced ground settlement was estimated over just the area covered by ejecta. This detailed examination of each case history provides a more robust estimate of ejecta-induced settlement than the rough estimates available previously. Each site was also characterized well by CPTs and other subsurface data.

The Hutabarat and Bray (2022) CPT-based $L_D - C_R$ chart was used to categorize the severity of the ejecta into the categories of None, Minor-Moderate, and Severe-Extreme. Categories were combined because the scatter in the localized ejecta-induced settlement case histories data did not justify the use of five distinct categories. The Mijic et al. (2022) free-field, level ground localized ejecta-induced ground settlement ranges of the three categories are shown in Table 2. The TPR is 79% for the Hutabarat and Bray (2022) estimate of 0 settlement for the 132 cases categorized as None in their $L_D - C_R$ chart; the TPR is 85% for their estimate of ≤50 mm settlement for the 48 cases categorized as Minor-Moderate; and the TPR is 71% for their estimate of 30-200-mm settlement for the 45 cases categorized as Severe-Extreme. Thus, the Hutabarat and Bray (2022) CPT-based ejecta severity chart designations of None, Minor-Moderate, and Severe-Extreme enable the engineer to estimate the free-field, level-ground, ejecta-induced settlement as either negligible, less than 50 mm, or 30-200 mm, respectively.

Table 2 should be used to estimate ejecta-induced ground settlement in most cases, because of the relative quality of the data of the Mijic et al. (2022) study. The Tonkin & Taylor localized

Table 2. Ejecta-induced settlement estimate

Ejecta severity category ^a	Estimated localized free-field ejecta-induced ground settlement ^b (mm)
None	0
Minor-moderate	≤ 50
Severe-extreme	30–200

^aHutabarat and Bray (2022) ejecta severity chart (Fig. 11) category. ^bLevel-ground ejecta-induced settlement estimated by Mijic et al. (2022).

ejecta-settlement estimates of Table 1 are conservative. However, the values in Tables 1 and 2 should be considered when estimating localized building settlement resulting from a defect in the crust or an adverse building foundation condition, because the values in Tables 1 and 2 bound the potential amount of localized ejecta-induced building settlement.

Site Characterization to Capture Element and System Responses

Depositional Environment

The role of depositional environment should be considered in liquefaction assessments. Youd and Perkins (1978) recognized depositional environment as a key factor affecting liquefaction-induced ground failure. They emphasized the importance of considering the sedimentation process, age of deposition, and geologic history. Seed (1979) highlighted the effects of soil fabric, overconsolidation ratio (OCR), and time under sustained loading. Laboratory testing by Ladd (1977) and Mulilis et al. (1977) showed that different soil fabrics can change the CRR of sand test specimens with the same D_r by a factor of two. Seed (1979) recommended obtaining the "best possible undisturbed samples" and using considerable judgement to interpret how the characteristics of those samples will affect in situ liquefaction behavior of the deposit. Additionally, Seed (1979) noted that even "a single layer of relatively impervious fine sand or silt ... would completely invalidate the results of pore pressure dissipation computations for vertical flow." The findings from recent studies of system response (e.g., Cubrinovski et al. 2018b; Beyzaei et al. 2018a, b; Hutabarat and Bray 2021a, b) also highlight the need to consider system response effects in conducting site investigations, laboratory tests, and analyses involving liquefaction.

Site Characterization Tools

Each project should start with a geologic assessment of the site and its surroundings. Much can be learned through the study of historical geologic maps and the evolution of the site (i.e., its depositional environment). For example, the 1850 geologic maps of Christchurch identified several streams that were buried as the city was developed, which liquefied in the 2011 Christchurch earthquake. Many of the zones of extensive liquefaction ejecta were located where old geologic maps depicted streams (e.g., Cubrinovski et al. 2011; Bray et al. 2014b; Beyzaei et al. 2018a). Geophysical tests should follow with the great insights that are possible through measurements of shear wave velocity (V_s) and compression wave velocity (V_p) , among other parameters. Subsurface explorations can follow to characterize the soil units that preliminary analyses indicate are likely to govern the seismic performance of the site.

Due to its repeatability and nearly continuous measurements, the CPT is superior to the standard penetration test (SPT) in characterizing the state of sand, silty sand, nonplastic silt, and low-plasticity clayey silts that may be susceptible to liquefaction. The CPT has also been used successfully in sandy gravels with at least 30% sand (e.g., Bray et al. 2014a; Dhakal et al. 2022). The CPT provides a nearly continuous robust measurement of cone tip resistance (q_t) , sleeve friction (f_s) , and pore-water pressure (u_2) , which are used to capture the response of soil to the penetration test. Measurement of V_s is also possible with the seismic CPT (SCPT) to capture the small strain stiffness of soil. The q_t and the derived parameters I_c and I_B characterize the state, response, compressibility, and strength of the soils penetrated by the CPT. I_c is superior to FC in characterizing soil compressibility (i.e., its effect on penetration

resistance), so it is preferred. Estimating FC based on I_c is highly uncertain. Closely spaced high-quality sampling and CPTs by Beyzaei et al. (2020) confirmed conclusively there are large variations in FC in samples directly adjacent to zones with nearly constant I_c values in laterally consistent soil profiles. Additionally, numerous validated CPT correlations are available to estimate ψ_o , D_r , s_u , k_v , etc. (e.g., Robertson and Cabal 2015), in addition to CRR (e.g., Boulanger and Idriss 2016). Some disturbed soil samples should be retrieved for soil index testing to evaluate liquefaction susceptibility of intermediate soils (e.g., using the PI \leq 12 and w/LL \geq 0.85 criteria). It is insightful to perform field vane shear tests (FVST) to explore peak and remolded strength of clayey soils that may be susceptible to strength loss.

High-quality "undisturbed" soil sampling of key soil units is prudent, especially for testing intermediate soils that are not well captured in the empirical database of the simplified liquefaction triggering procedures. The Dames & Moore (DM) hydraulic fixed-piston thin-walled tube sampler can retrieve high-quality samples of silt and silty sand (Markham et al. 2016), especially if the soil contains some clayey materials (Bray and Sancio 2006). As noted by Bray and Sancio (2008) and Boulanger and Idriss (2008), clayey silt soil can be sampled effectively. Cyclic testing can capture the cyclic response of these soils, which is invaluable for gaining insight on their likely performance and calibrating soil constitutive models to support dynamic nonlinear effective stress analysis.

There is also value in performing high-quality continuous sampling to characterize geologic details and evidence of important features of depositional environment that are lost with conventional sampling. For instance, CPT, mini-CPT, and sonic borings did not adequately capture thin layering and soil fabric in Christchurch (Beyzaei et al. 2020). Conversely, detailed logging of high-quality samples captured the actual in situ layering at silty soil sites that did not manifest liquefaction even though simplified liquefaction triggering procedures indicated they would at the Canterbury earthquake levels of shaking. Scanning electron microscope (SEM) images were useful to see the soil and potentially key characteristics not identified previously, such as soil fabric, cementation, and

particle shape. Additionally, multiple groundwater measurement methods (e.g., piezometers, high-quality sampling, V_p testing, and regional groundwater maps) were required to characterize complex groundwater conditions, including groundwater fluctuations.

Illustrative Example

Ground improvement was required to mitigate liquefaction effects to develop areas of Treasure Island, San Francisco, California. Simplified CPT-based liquefaction triggering methods indicated that the entire surficial cohesionless soil deposit overlying the Young Bay mud at the site would liquefy during the design events. A test program was performed to evaluate the effectiveness of improving the liquefiable deposit with vibro-compaction by using direct power compaction (DPC) equipment (ENGEO 2016). Before ground improvement, CPT tip resistances of the soil deposit are shown with the blue traces in Fig. 12(a) in four cells of the ground improvement trials. The post-DPC CPT resistances are shown in red and green traces for CPTs performed 17 days and 31 days, respectively, after attempting to densify the surficial cohesionless soil deposit. The upper half of this unit was densified satisfactorily, as evidenced by the significant increase in its q_c values. CPT tip resistances did not increase in the lower half of the unit. Application of the Robertson (2016) approach to differentiate soils with microstructure (e.g., cementation/bonding and aging) from "ideal soils" (e.g., young and uncemented) through the K_G^* parameter did not discern significant differences between the upper half and lower half of the unit, as shown in Fig. 12(b).

DM sampling of the soil deposit was conducted to retrieve high-quality samples for CSS testing and to log in detail (ENGEO 2016). The upper half of the unit was clearly identified visually as clean sand fill with few nonplastic fines. It was loose, young, and uncemented. Vibro-compaction effectively densified this material as expected. High-quality samples of the lower half of the unit revealed that it was a highly reworked heterogeneous natural sandy shoal deposit with interlocking sand grains with clay bridges, as shown in Fig. 13. There was close grain packing with clay films bridging pores. At times, the clay bridges were weakly developed with fewer

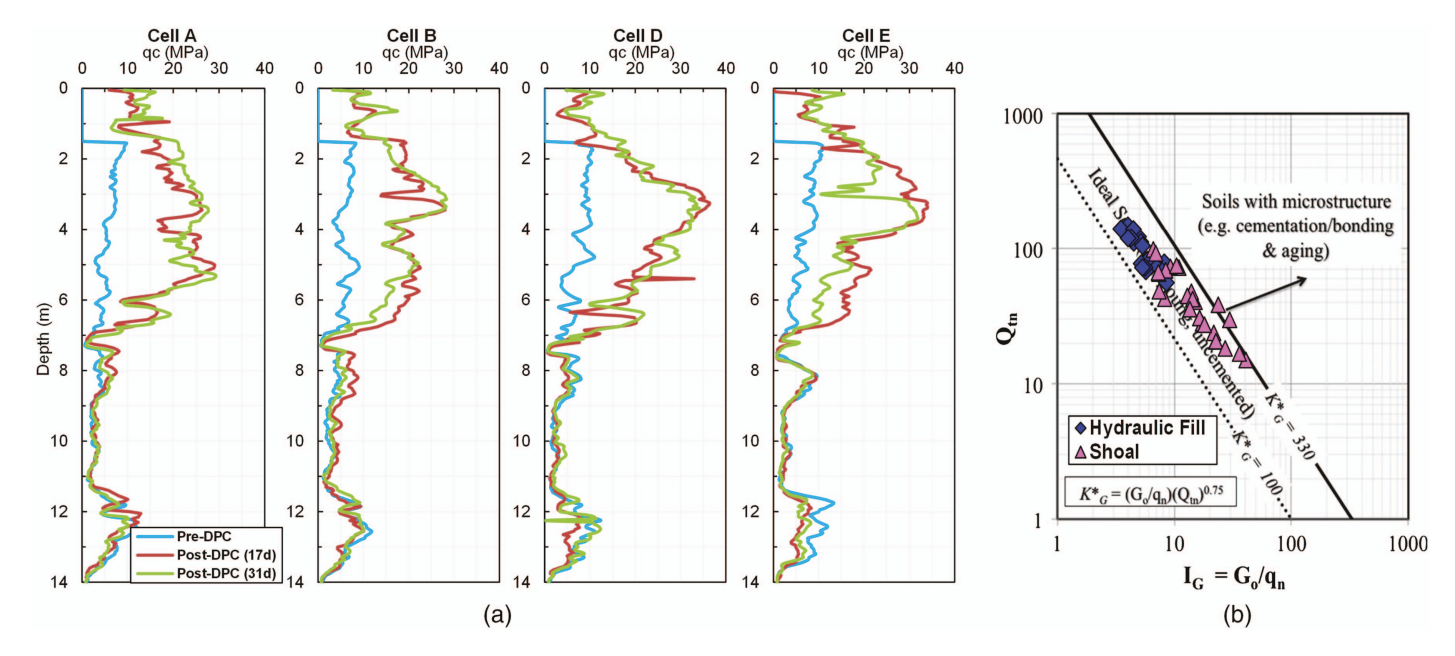


Fig. 12. (Color) In situ characterization of the fill-shoal material at the ground improvement trial site at Treasure Island: (a) pre-DPC and post-DPC treatment CPTu profiles; and (b) data plotted on the Robertson (2016) Q_{in} – I_G microstructure chart. (Data from ENGEO 2016.)

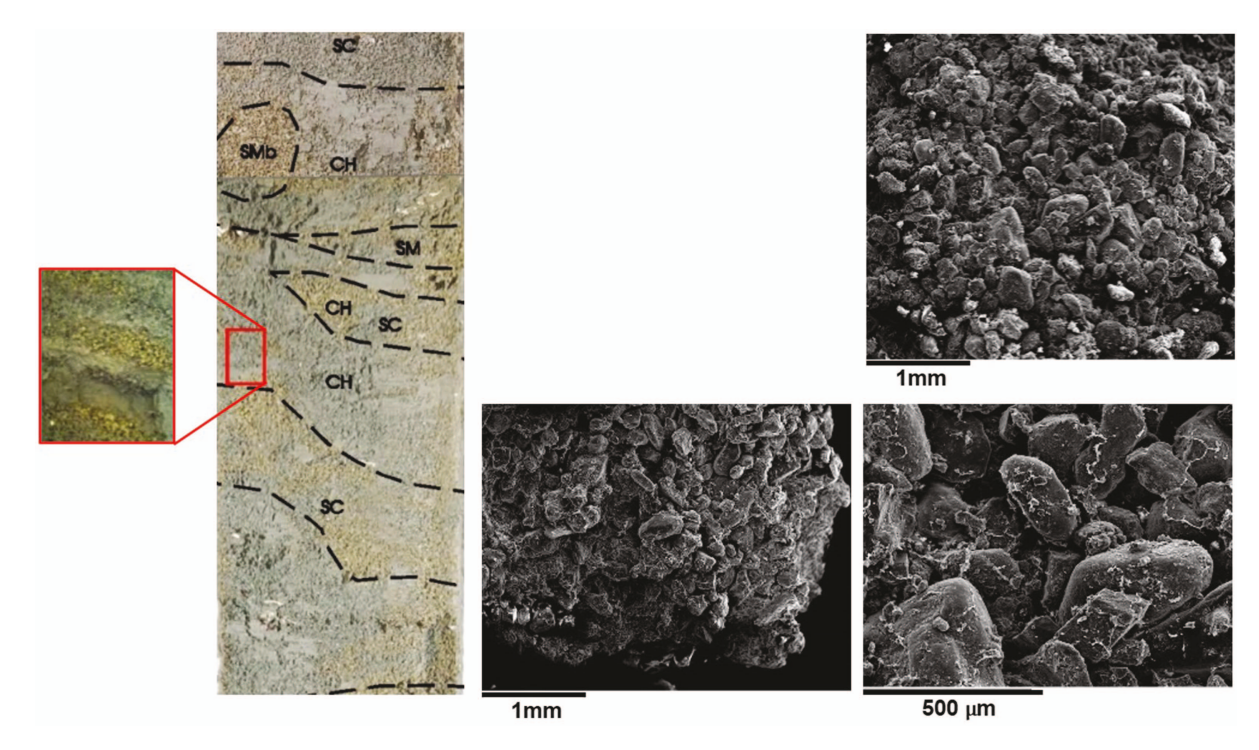


Fig. 13. (Color) Detailed mapping of high-quality DM sample retrieved from Treasure Island shoal deposit (~11.1-m depth) with SEM images showing its fabric (~9.4 m). (Data from ENGEO 2016.)

fines, but the sand-size particles were packed into a stable arrangement of "interacting blocks" fabric as shown in the SEM images of Fig. 13. The DPC equipment could not densify the natural shoal deposit because this deposit had a fabric that resisted densification through vibration. It was also more resistant to cyclic loading than the CPT-based simplified liquefaction-triggering procedures indicated. High-quality continuous sampling provided engineers with the information and insights required to consider these key issues in their evaluation of the seismic performance of the site.

Postliquefaction Volumetric-Induced Ground Settlement

Motivation

Deterministic CPT-based postliquefaction ground settlement procedures are widely used in practice (e.g., Zhang et al. 2002; Idriss and Boulanger 2008). A probabilistic CPT-based postliquefaction ground settlement procedure is required in support of performancebased earthquake engineering. Cetin et al. (2009) developed a probabilistic SPT-based postliquefaction ground settlement procedure, but the CPT is superior to the SPT, as discussed previously. Therefore, a probabilistic CPT-based postliquefaction ground settlement procedure for free-field level ground conditions is developed. It takes advantage of the results of a comprehensive database of laboratory tests with postcyclic volumetric reconsolidation (Olaya and Bray 2022b) and a comprehensive database of field case histories of sites undergoing postliquefaction volumetric-induced ground settlement (Olaya and Bray 2022a). In contrast, several of the current CPT-based postliquefaction ground-settlement procedures have comparisons against a limited number of case histories, and they are based solely on the Ishihara and Yoshimine (1992) family of curves derived from CSS tests performed on one uniform clean sand (i.e., Fuji River Sand with FC = 0%, $e_{\text{max}} = 1.064$, $e_{\rm min}=0.529$, coefficient of uniformity, $C_u=3.2$, and median grain size, $D_{50}=0.4$ mm) reconstituted to three different relative densities (47%, 73%, and 93%) and tested at one vertical effective confining stress (196 kPa). Although these methods have been shown to produce reasonable results, it has not been determined if the relationships developed from test data on just one uniform clean sand can be applied to other clean sands with other particle shapes and gradations, nonplastic silty sands, and nonplastic silts (Bray et al. 2017).

Postliquefaction Laboratory Tests

Olaya and Bray (2022b) developed a database of 579 test results on postliquefaction volumetric strain (ε_v) , including 299 test results that relate maximum shear strain (γ_{max}) to the factor of safety against liquefaction triggering (FS_L) . The database includes postcyclic test data on 10 clean sands, 2 gravels, 3 silty sands, 5 silts, and 3 clayey soils. The results of the numerous cyclic tests on a wide range of soil types enabled key trends of the effects of state, stress, soil type, gradation, etc. on the development of postliquefaction volumetric strain to be identified. Their study found that uniform clean sand, gravel, nonplastic silty sand, and nonplastic silt test results could be captured in a unified manner using either D_r , ψ_o , or e_o to characterize the state of the soil. Postliquefaction volumetric strain depended primarily on the state of the soil and the induced $\gamma_{\rm max}.$ The type of loading or effective confining stress (within the range of 40-400 kPa) were less important. Olaya and Bray (2022b) developed models using either D_r , ψ_o , or e_o as the independent variable to estimate ε_v for uniform clean sand, nonplastic silty sand, and nonplastic silt with quantification of the uncertainty of the estimate of volumetric strain. They also developed new models that estimate γ_{\max} as a function of FS_L for uniform clean sand, nonplastic silty sand, and nonplastic silt with quantification of the uncertainty of the estimate. These experimentally based models can be used to inform the characteristics of an

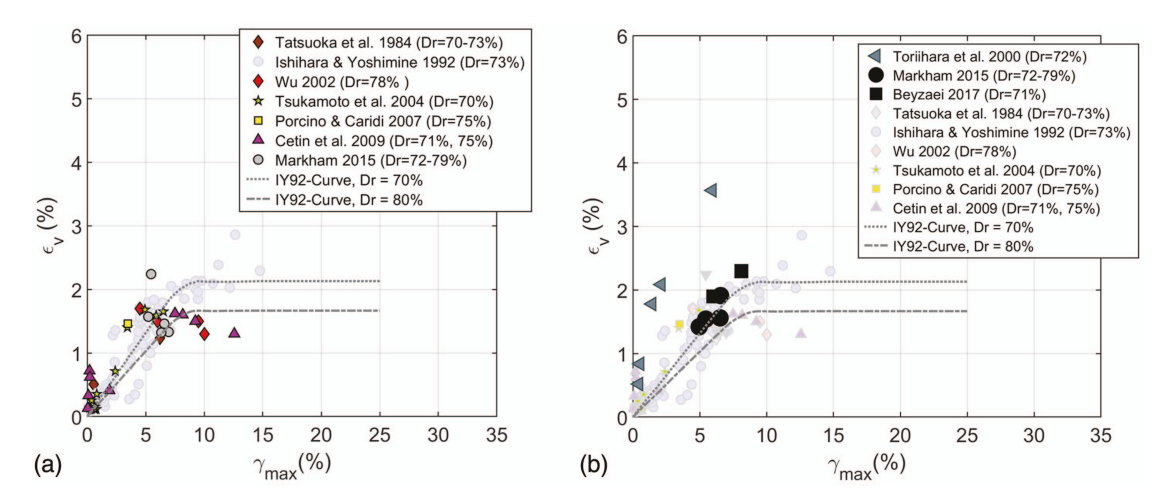


Fig. 14. (Color) Volumetric strain versus maximum shear stress test data for $D_r = 70\%$ –80%: (a) clean uniform sand [Ishihara and Yoshimine (1992) clean sand data are shown as light data points]; and (b) nonplastic to low-plasticity silty sand (clean uniform sand data shown as light data points). (Reprinted from Olaya and Bray 2022b, © ASCE.)

empirical CPT-based postliquefaction model used to fit the case history data.

Like Ishihara and Yoshimine (1992) and several other researchers examining uniform sand data, D_r was examined first as the independent variable to characterize the state of the uniform nonplastic soil. Only nonplastic soils with $C_u < 4$ were considered because D_r has been shown to be a reasonable parameter for comparing the state of different nonplastic soils if they are of uniform gradation. For instance, Bolton (1986) showed that the shear response of different clean sands can be grouped and characterized using D_r , provided these sands are of similar uniform gradations. Duncan et al. (2014) also showed D_r is an efficient parameter for characterizing the strength of granular materials of sands with similar C_u values. Whang (2001) analyzed seismically induced compression of different sands using D_r , and Duku et al. (2008) combined 16 different sands using D_r to develop a seismic compression model applicable to a broad range of uniform sands. As discussed previously, Cubrinovski (2019) found that D_r could be used to assess the liquefaction potential of nonplastic silty sand and tied directly to the D_r of uniform clean sand to compare responses of different soil types. Mijic et al. (2021a) also found comparable soil responses for uniform clean sand, uniform nonplastic silty sand, and uniform nonplastic silt with FC up to 70%.

Postliquefaction Volumetric Strain Models

Use of D_r enabled confirmation that uniform clean sands and uniform nonplastic silty sands at the same D_r under the same effective confining stress and sheared to the same $\gamma_{\rm max}$ develop similar ε_v , as shown in Fig. 14 (Olaya and Bray 2022b). All clean-sand data shown in Fig. 14(a) and silty-sand data shown in Fig. 14(b) with $C_u < 4$ exhibit consistent responses. The only data that are inconsistent with the overall trends are tests by Toriihara et al. (2000), conducted on sand with compressible/crushable fine soil matrix with $C_u = 18$ [shown in Fig. 14(b)]. Similarly, uniform sand, uniform nonplastic silty sand, and uniform nonplastic silt test specimens at the same ψ_o develop similar ε_v when sheared to the same $\gamma_{\rm max}$ (Olaya and Bray 2022b).

Olaya and Bray (2022b) performed a series of nonlinear regression analyses of the uniform nonplastic soil data using different functional forms, first over the entire dataset and then over individual 10% bins of D_r (e.g., 50% to 60%) to find an efficient and

sufficient model. For a specific D_r bin of test results, ε_v increases directly proportional to $\gamma_{\rm max}$ until it becomes constant at $\gamma_{\rm max} > 8\%$. The resulting model to estimate ε_v (in %) as function of $\gamma_{\rm max}$ (in %) for a specified value of D_r (in decimal) is

$$\varepsilon_v = 1.14 \cdot \exp(-2.0 \cdot D_r) \cdot \min(\gamma_{\text{max}}, 8\%) \cdot e^{\varepsilon}$$
 (4)

where ε = model residuals that are normally distributed and unbiased with zero mean with $\sigma = 0.62$ in natural log units. The variability in estimating ε_v includes within-material testing variability and between-material variability. High-quality, extensive testing of just one material had lower variability [e.g., $\sigma = 0.36$ and 0.41 for the Ishihara and Yoshimine (1992) and Shamoto et al. (1996) datasets, respectively]. Thus, the σ in Eq. (4) could be reduced if sufficient ε_v data on a specific soil are available; however, its bias from the median estimate for that material would need to be considered. The Olaya and Bray (2022b) bilinear model and the $\pm 1\sigma$ range for $D_r = 70\%$ –80% are illustrated in Fig. 15(a), where the observed data trends are captured well. The proposed model contours for D_r values from 30% to 90% are shown in Fig. 15(b) along with the Ishihara and Yoshimine (1992) clean sand curves for comparison. The results of the regression analyses using the enlarged database indicate that ε_v varies within a slightly narrower range than envisioned previously. It is important to capture these variations in ε_v in CPT procedures that track changes of D_r in a soil deposit.

Although the initial state parameter captures the volumetric strain potential of uniform clean sand, silty sand, and nonplastic silt in a unified manner, the ψ_o data are only one-fifth of the D_r data because the SSL is not determined in most testing programs (Olaya and Bray 2022b). Accordingly, the ψ_o model is preliminary. Additionally, there is greater uncertainty in estimating ψ_o in situ relative to estimating D_r . The model developed to estimate ε_v (in %) as function of $\gamma_{\rm max}$ (in %) for a specified value of ψ_o (in decimal) is

$$\varepsilon_v = 0.50 \cdot \exp(4.0 \cdot \psi_o) \cdot \min(\gamma_{\text{max}}, 8\%) \cdot e^{\varepsilon} \tag{5}$$

The model residuals are zero mean normally distributed with $\sigma=0.56$ in natural log units. The proposed bilinear model and the $\pm 1\sigma$ range for $\psi_o=-0.15$ to -0.10 are illustrated in Fig. 16(a), where the observed data trends are captured well. The proposed model contours for ψ_o values from -0.25 to 0.05 are shown in

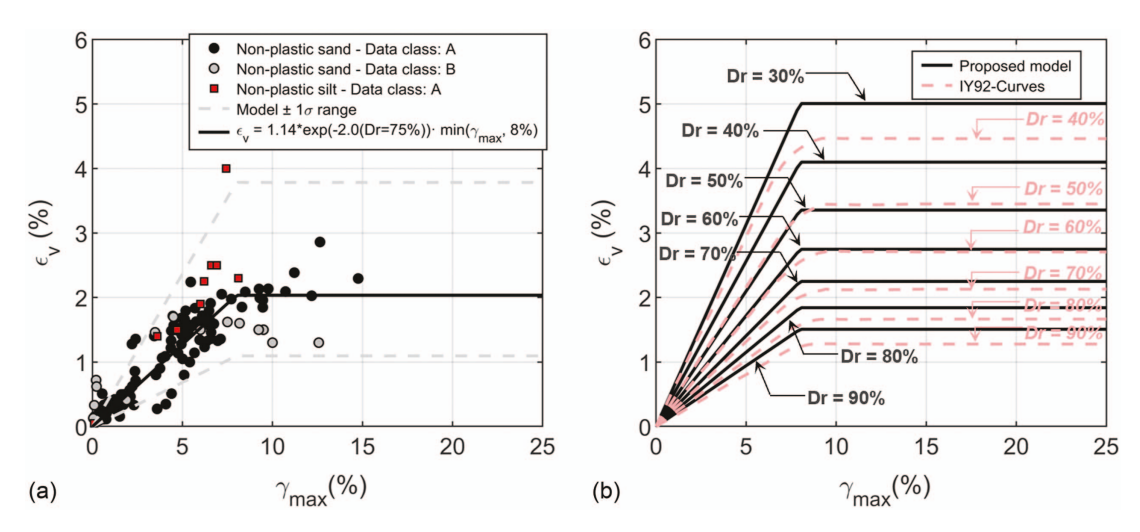


Fig. 15. (Color) Nonplastic uniform soil ε_v - $\gamma_{\rm max}$ proposed model in terms relative density: (a) $D_r = 70\%$ -80%; and (b) model contours. (Reprinted from Olaya and Bray 2022b, © ASCE.)

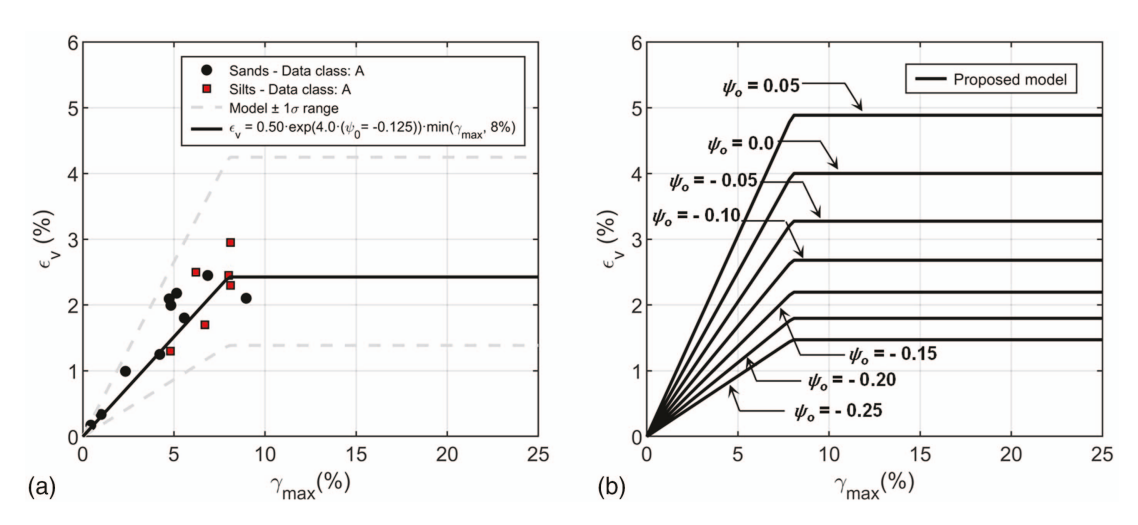


Fig. 16. (Color) Nonplastic uniform soil ε_v - $\gamma_{\rm max}$ proposed model in terms of state parameter: (a) $\psi_o = -0.15$ to -0.10; and (b) model contours. (Reprinted from Olaya and Bray 2022b, © ASCE.)

Fig. 16(b). Like the D_r -based models, the maximum ε_v varies within a range of about 1.5% to about 5% for the range of test data available. Overall, the ψ_o -based model performs reasonably well considering the limitations of the data (Olaya and Bray 2022b). Experimental programs should establish the SSL of the tested soil to enable ψ_o -based models to be refined.

Maximum Shear Strain Potential Models

Ishihara and Yoshimine (1992) recognized that initial liquefaction was triggered ($FS_L=1.0$) in numerous CSS tests at a single-amplitude shear strain ($\gamma_{cyc,SA}$) of about 3.5%, which is consistent with the 5% double-amplitude axial strain ($\gamma_{cyc,DA}$) criterion often used with CTX tests. They also noted an inverse relationship between FS_L and $\gamma_{\rm max}$. Initial regressions of the enlarged Olaya and Bray (2022b) database indicated that a hyperbolic relationship captures the $FS_L - \gamma_{\rm max}$ data trends well. To avoid having $FS_L - \varepsilon_v$ curves at different D_r values cross when relating FS_L and strain potential, the model requires slightly different curvature once $FS_L=1.0$ is crossed. Their hyperbolic model depends on one parameter (A) that is a function of D_r (in decimal) as

$$\gamma_{\text{max}} = 3.5 \cdot \left[\frac{2^A - FS_L^A}{2^A - 1} \right] \cdot e^{\varepsilon}$$

$$\gamma_{\text{max}} = 0; \quad \text{for } FS_L \ge 2.0$$
(6)

where

$$A = \begin{cases} -2.8 \cdot D_r^2 + 10.2 \cdot D_r - 9.8; & FS_L \ge 1.0 \\ -275 \cdot \exp(-6.6 \cdot D_r); & FS_L < 1.0 \end{cases}$$

The model residuals (ε) are zero mean normally distributed with $\sigma=0.88$ in natural log units. The proposed $FS_L-\gamma_{\rm max}$ model for the $D_r=40\%-50\%$ bin is shown in Fig. 17 with the Yoshimine et al. (2006) model for comparison. The additional test data and the Ishihara and Yoshimine (1992) data show similar scatter, with the Olaya and Bray (2022b) model deviating slightly from the Yoshimine et al. (2006) model. Differences in the models are larger for denser soils. There are not enough ψ_o data available to develop a robust $FS_L-\gamma_{\rm max}$ model for ψ_o . Olaya and Bray (2022b) developed a relationship to link ψ_o to D_r , so the D_r -based $FS_L-\gamma_{\rm max}$ is used

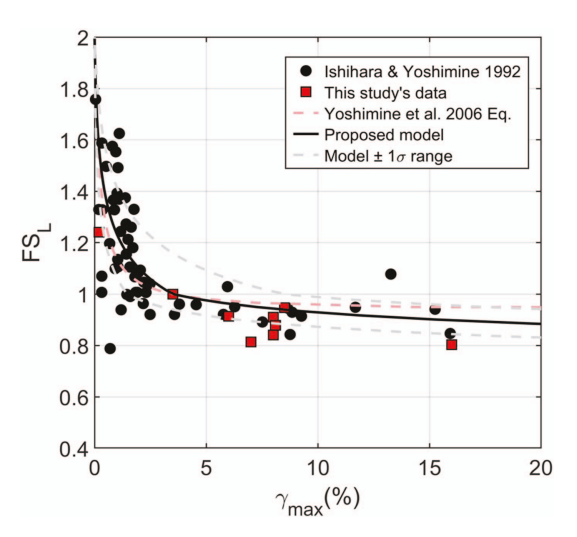


Fig. 17. (Color) γ_{max} – FS_L data and proposed model in terms relative density for $D_r = 40\%$ –50%. (Reprinted from Olaya and Bray 2022b, © ASCE.)

with the ψ_o -based $\gamma_{\rm max}$ - ε_v model to estimate postliquefaction volumetric strain, which requires $\gamma_{\rm max}$ as an input.

Relating FS_L and Volumetric Strain Potential

Ishihara and Yoshimine (1992) developed a widely used figure to estimate ε_v or $\gamma_{\rm max}$ versus FS_L as a function of a sand's D_r to estimate liquefaction-induced ground settlement or lateral spreading. The Olaya and Bray (2022b) models discussed previously provide alternative estimates of ε_v and $\gamma_{\rm max}$ using either D_r or ψ_o as a measure of the soil's state and FS_L as a proxy for the seismic demand. These models can be combined to estimate postliquefaction volumetric-induced free-field ground settlement in a consistent manner. The models defined by Eqs. (4) and (6) describe the relationship between ε_v and FS_L as a function of D_r , as shown in Fig. 18. Importantly, the combined equations provide D_r curves that do not cross, unlike other models.

Probabilistic CPT-Based Liquefaction Ground-Settlement Procedure

Postliquefaction Ground-Settlement Field Case Histories

Postliquefaction-induced ground settlement is a complex process resulting from the combined effects of particle sedimentation and soil reconsolidation due to postshaking dissipation of excess pore-water pressure. Available CPT-based empirical models to estimate liquefaction-induced settlement for free-field level ground conditions are based on a limited number of field case histories. Consequently, it is difficult to quantify uncertainty in the estimate of postliquefaction settlement with the limited number of field case histories available. To remedy this deficiency, Olaya and Bray (2022a) developed a database of 205 well-documented groundsettlement case histories to support the development of an improved probabilistic CPT-based liquefaction-induced ground-settlement procedure. Their study takes advantage of the numerous site investigations, ground motion recordings, and LiDAR surveys performed following the 2010-2011 Canterbury earthquake sequence and the 2013-2016 northern South Island, New Zealand, earthquakes.

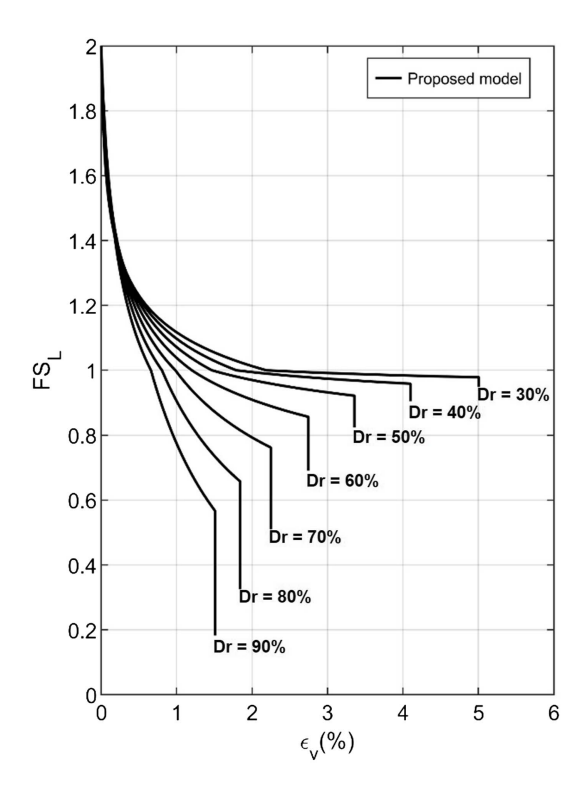


Fig. 18. Relationship between ε_v and FS_L in terms of D_r . (Reprinted from Olaya and Bray 2022b, © ASCE.)

Obtaining field case histories with reliable pre- and postearthquake ground surface elevation measurements is the primary limitation in the development of postliquefaction ground-settlement case histories. CPT-based investigations and topographic surveys conducted by the US Geological Survey (USGS) following the 1989 Loma Prieta earthquake produced some of the first CPT-based well-documented case histories of postliquefaction settlement. Additional case histories have gradually become available. However, the reconnaissance efforts conducted in Christchurch after the 2010-2011 Canterbury earthquakes produced an unparalleled amount of diverse and high-quality data with ground motion recordings, ground performance observations for four major earthquakes, aerial imagery, LiDAR measurements, and subsurface characterization, largely through CPTs. Research teams developed an initial set of 55 welldocumented sites to investigate cases where none-to-minor land damage was observed, even though simplified liquefaction methods estimated severe surface manifestations (e.g., Russell and van Ballegoy 2015; Cubrinovski et al. 2018b). Mijic et al. (2022) developed 34 additional sites with the goal of including sites with and without liquefaction manifestations that show no major discrepancies between the estimates from simplified liquefaction methods and the actual field observations. Free-field level ground sites in these two datasets were examined to enlarge the postliquefaction ground-settlement database. Additionally, well-documented sites in Wellington, New Zealand, that experienced three major earthquakes, including the 2016 Kaikoura earthquake, were added to the Olaya and Bray (2022a) database. The final compilation of free-field level-ground postliquefaction settlement case histories by Olaya and Bray (2022a) is summarized in Table 3. There are 205 case histories at sites described by 967 CPTs with reliable ground-settlement measurements.

Olaya and Bray (2022a) defined a case history as the combination of (1) a site with laterally uniform soil stratigraphy with at least one CPT, (2) an earthquake event represented by its M_w , ground

Table 3. Summary of free-field settlement case histories

Location	Earthquake	Case histories	CPTs	Type of deposit
Marina District, California	1989 Loma Prieta	4	8	Hydraulic fill
Treasure Island, California		5	84	•
Wufeng, Taiwan	1999 Chi-Chi	3	3	Natural soil
Yuanlin, Taiwan		3	4	
CentrePort, Wellington	2013 Cook Strait	1	8	Hydraulic fill
	2013 Lake Grassmere	13	69	·
	2016 Kaikoura	13	69	
Christchurch, New Zealand	2010 Darfield	45	210	Natural soil
	2011 Christchurch	47	220	
	2011 June	65	285	
Urayasu, Japan	2011 Tohoku	6	6	Hydraulic fill
	Total	205	967	

Source: Reprinted from Olaya and Bray (2022a), with permission.

surface PGA, or other intensity measures, and (3) consistent post-liquefaction volumetric-induced free-field level-ground settlement measurements. A site is not defined by a CPT. Instead, a site is defined by its consistent geology and seismic performance. Thus, each case history is a site characterized by a geometric mean set of CPT-derived parameters, which undergoes an estimated level of earthquake shaking, wherein the liquefaction-induced ground settlement was measured. Sites characterized with several CPTs are valuable because they capture the average subsurface conditions and the variability of the CPT parameters across a site. For sites with multiple CPT soundings or multiple point settlement measurements, geometric means of these values are used to represent central values in the case history.

An illustrative definition of a case history is depicted in Fig. 19. The stratigraphy, soil types, and the effects of liquefaction experienced at CentrePort in Wellington after the 2013 Cook Strait, 2013 Lake Grassmere, and 2016 Kaikoura earthquakes have been documented extensively (e.g., Cubrinovski et al. 2018a; Dhakal et al. 2020, 2022). CPT data were collected through a collaborative research effort led by the University of Canterbury with the University of California, Berkeley, Tonkin & Taylor, Ltd., and CentrePort. Site 4 is within a part of CentrePort built with dumped sandy gravel

fill. The sand-silt fractions of the gravelly fill are between 30% and 70%. The CPT data (e.g., q_{c1n} , I_c .) and liquefaction parameters (e.g., FS_L and LSN) were used to define the extent of a site. They are relatively consistent for the 6 CPTs advanced in Site 4. Additionally, the surveyed ground settlement varies between 200 and 350 mm across most of the site. Last, the M_w of the earthquake events are known, and PGA can be estimated with confidence with nearby strong motion stations that are not affected by liquefaction.

Reclaimed land is typically the product of sequential hydraulic filling of borrowed granular material. This construction method results in relatively uniform and loose fills typically overlying marine sediments. The hydraulic fills in the database are usually less than 10-m thick and are typically comprised of silty sands to sandy silts (with exception of CentrePort, which has a significant fraction of gravel). Case histories of the performance of hydraulic fills, such as those during the 1995 Kobe earthquake (e.g., Yasuda et al. 1996), indicate that uniformly constructed hydraulic fills tend to exhibit relatively uniform settlement. Conversely, natural soil deposits are inherently heterogenous because of complex depositional processes that can show significant spatial variability in addition to other age-related effects. The assessment of liquefaction performance in Christchurch illustrates the effects of depositional

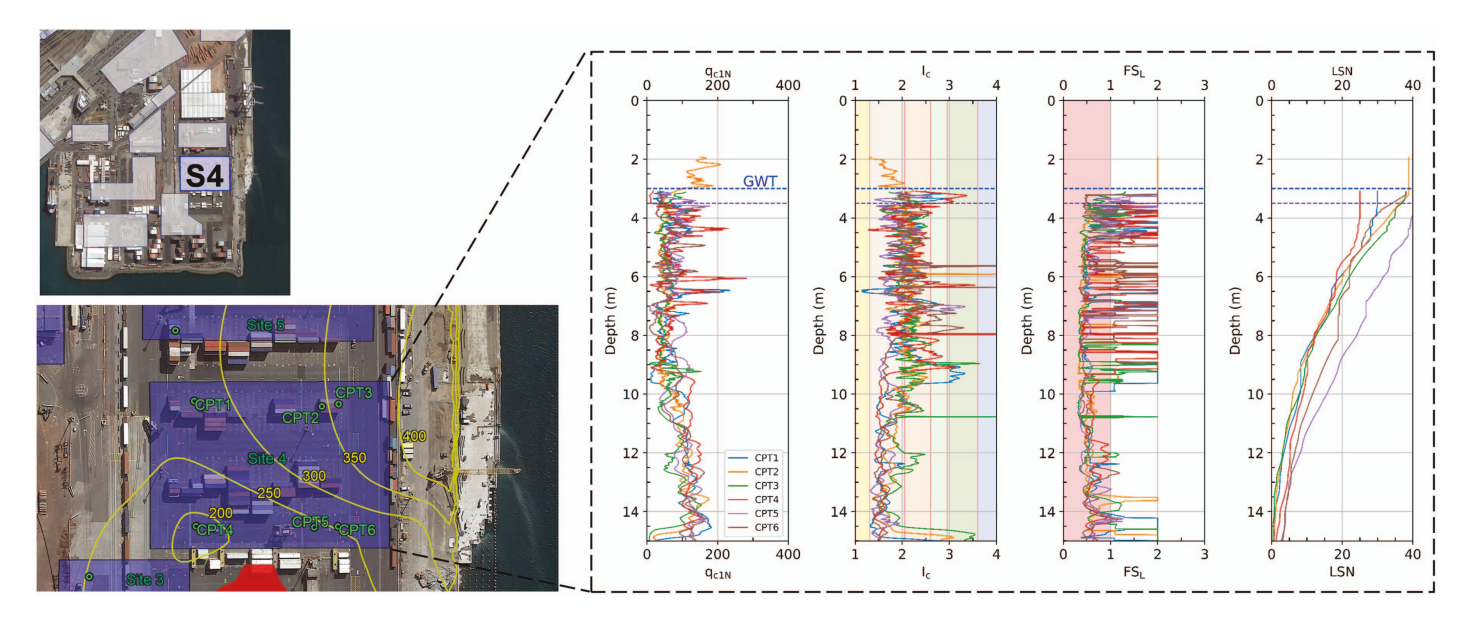


Fig. 19. (Color) CentrePort with enlarged image of Site 4 showing CPT locations and mean ground settlement (mm) contours with q_{cln} , I_c , FS_L , and LSN profiles. (Data from Dhakal et al. 2022; Olaya and Bray 2022a; base images © Google Earth.)

processes on ground performance (Beyzaei et al. 2018b). Due to their differing formation processes and seismic performance, the case histories are classified into the two primary categories of natural soil deposits and hydraulic fills. Of the 205 case histories, 163 cases are natural soil deposits and 42 cases are hydraulic fills.

Framework of the Procedure

The proposed probabilistic CPT-based liquefaction ground-settlement procedure employs the framework of Ishihara and Yoshimine (1992), which is the framework used in several existing procedures (e.g., Zhang et al. 2002; Idriss and Boulanger 2008). The postliquefaction volumetric ground settlement (S_v) is calculated initially as

$$S_v = \sum_i \varepsilon_{v_i} \cdot \Delta Z_i \tag{7}$$

where ε_{v_i} = median postliquefaction volumetric strain calculated using the Olaya and Bray (2022b) model for all nonplastic soils, which is calculated using either its D_r -based or ψ_o -based FS_{L} - $\gamma_{\rm max}$ and $\gamma_{\rm max}$ - ε_v relationships in which FS_L and D_r or ψ_o are estimated using CPT data at each depth i; and ΔZ_i = thickness of the unit at depth i. The procedure was developed using the mean FS_L at a probability of liquefaction triggering (P_L) of 50% calculated using two simplified liquefaction triggering procedures: (1) the Robertson and Wride (1998) procedure as updated by Robertson (2009) and converted to a probabilistic method by Ku et al. (2012), and (2) the Boulanger and Idriss (2016) procedure. The intent is to use an unbiased mean-centered estimate of FS_L . Using $P_L = 15\%$ instead of $P_L = 50\%$ produces a conservative estimate of S_v . Use of one simplified liquefaction procedure or alternative procedures changes the estimate of FS_L in a manner dependent on the procedure(s) employed.

The proposed postliquefaction ground-settlement procedure also requires a CPT-based estimate of D_r or ψ_o . CPT-based correlations to estimate D_r are based on clean sand data (e.g., Tatsuoka et al. 1990). Correlations to estimate D_r as a function of CPT data in silty soil do not exist. To address this shortcoming, D_r data of high-quality DM nonplastic soil samples retrieved by Markham (2015) and Beyzaei (2017) within 2 m of CPTs in Christchurch were compiled and examined. These data are shown in Fig. 20 in terms of q_{c1n}/D_r^2 versus I_c . The q_{c1n}/D_r^2 relationship is widely used for clean sand (Robertson and Cabal 2015). The data in Fig. 20 enable it to be used for silty soils as a function of soil compressibility represented by I_c . The ratio q_{c1n}/D_r^2 decreases as soil compressibility increases (i.e., as I_c increases), because the CPT tip resistance decreases in more compressible soils if the soils have the same D_r . The proposed relationship was extended to capture sand with $I_c < 1.6$ using an average of the existing CPT-based D_r correlations for clean sand with $q_{c1n}/D_r^2 = 290$, as shown in Eq. (8) where D_r is expressed in decimal. The model residuals (ε) are zero mean normally distributed with $\sigma = 0.31$ in natural log units

$$D_r = \begin{cases} \sqrt{\frac{q_{c1n}}{290}} & \text{for } I_c < 1.6\\ \sqrt{\frac{q_{c1n} \cdot I_c^{3.5}}{1,500}} & \text{for } 1.6 \le I_c \le 2.6 \end{cases}$$
 (8)

As an alternative to the proposed model, the Robertson and Cabal (2015) CPT-based D_r correlation for clean sand is used. It is extended to capture silty soils with $I_c > 1.64$ using the clean sand correction factor (K_c) of Robertson and Wride (1998) with a

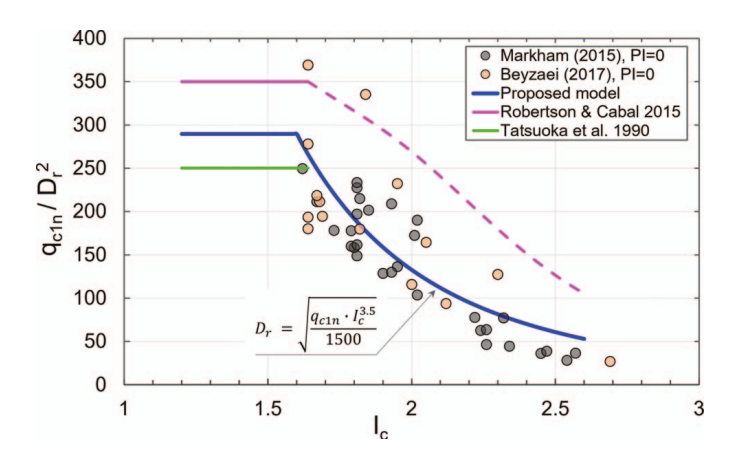


Fig. 20. (Color) Influence of soil compressibility (through I_c) on the ratio of CPT tip resistance to D_r^2 .

compressibility factor of 350. The resulting relationship is also shown in Fig. 20. Similar to what was done for FS_L , the average of the two D_r values estimated by these CPT correlations is used in the development of the postliquefaction ground-settlement procedure to develop a mean-centered estimate of D_r .

The average of two CPT-based correlations to estimate ψ_o is also used for the ψ_o -based volumetric strain model. Robertson (2010) developed a correlation to estimate ψ_o based on clean sand equivalent resistance ($Q_{tn,cs}$). As an alternative to this correlation, Olaya and Bray (2022b) developed a CPT correlation to estimate ψ_o based on clean sand and nonplastic silty sand and silt laboratory data with a generic SSL equation based on Bolton (1986) dilatancy index, resulting in estimating ψ_o as

$$\psi_o = e_o - e_{cs} = \xi \cdot (e_{\text{max}} - e_{\text{min}})[1/\ln(\sigma'_{cr}/\sigma'_{c}) - D_r]$$
 (9)

where D_r is in decimal; σ'_{cr} = soil's crushing stress; σ'_{c} = effective normal/confining stress; and ξ is introduced as an adjustment factor that accounts for the assumptions required to convert the Bolton (1986) equation into Eq. (9) and the variability of the individual relationships used to develop Eq. (9) (e.g., variability in estimation of $e_{\text{max}} - e_{\text{min}}$). The ξ factor was developed through a calibration process using data from 60 laboratory tests to account for the sources of error in the approximation of Eq. (9) as

$$\xi = 0.724 \cdot \exp(-0.031 \cdot FC) \tag{10}$$

where FC is expressed in percent as an integer. Examination of Eq. (9) showed that the estimate of ψ_o is not too sensitive to σ'_{cr} , so typical values provided by Mitchell and Soga (2005) are used (i.e., 8,000 kPa for silt; 10,000 kPa for silty sand; and 20,000 kPa for clean sand). The average of the soil-dependent correlation of Cubrinovski and Ishihara (2002) is used to estimate $e_{\rm max}-e_{\rm min}$ as

$$e_{\text{max}} - e_{\text{min}} = \begin{cases} 0.43 + 0.00867 \cdot FC, & FC < 30\\ 0.57 + 0.004 \cdot FC, & FC \ge 30 \end{cases}$$
(11)

where FC is expressed in percent as an integer. Typical values of $e_{\rm max}-e_{\rm min}$ are 0.45 for clean sand, 0.65 for silty sand, and 0.80 for silt.

Adjustments and Calibration of the Model

Residuals are calculated as $\ln(S_{v_meas}) - \ln(S_{v_est})$, where S_{v_meas} is the mean measured settlement and S_{v_est} is estimated from Eq. (7) using the median estimate of the Olaya and Bray (2022b) postlique-faction volumetric strain model presented previously. The residuals

obtained using Eq. (7) without adjustments are shown in Fig. 21. These residuals show differences between estimates for natural soil deposits and hydraulic fills as expected due to their different depositional processes. It is apparent that the laboratory-based model has different biases in its estimates of the settlement measured at natural soil deposit and hydraulic fill sites. In addition, evaluation of the distributions of the residuals shows bias as a function of a site's average I_c and bias as a function of the earthquake's M_w . Based on these observations, a calibration factor (C), a soil behavior factor (SB), and a magnitude factor (MF) are incorporated in the final model. The final regression analyses were performed considering the effects of C, SB, and MF simultaneously. However, the results of the initial data analyses that led to the development of these factors are informative and are discussed further in this section of the paper. The calibration and correction factors are developed using the D_r -based strain potential models [Eqs. (4) and (6)], and these factors are then applied to the ψ_a -based model because there is greater confidence at this time in the D_r -based model, which has more data and more established correlations to estimate D_r . Last, several depth-weighting factors (e.g., Cetin et al. 2009; van Ballegoy et al. 2014) were investigated, but a depth-weighting factor was not incorporated in the model because it did not reduce the standard deviation or the bias in the model. Moreover, sensitivity studies found that the use of a depth-weighting factor made mechanistically incorrect adjustments to the postliquefaction ground settlement estimate, as a liquefiable layer of variable thickness was moved up and down in simplified soil profiles.

The calibration factor C is the result of the constant overall offset observed in the residuals of clean-sand natural-soil sites represented by an average I_c value in the upper 15 m of the profile $(I_{c15}) < 1.8$. This factor is due to inherent differences between

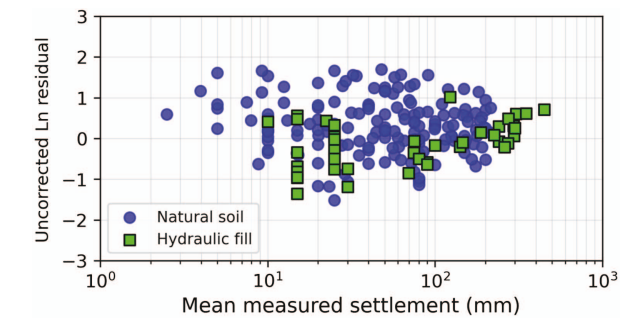


Fig. 21. (Color) Initial residuals $[\ln(S_{v_meas}) - \ln(S_{v_est})]$ using the Olaya and Bray (2022b) postliquefaction volumetric strain model without adjustments.

the characteristics of natural soil deposits and the largely reconstituted or slightly disturbed soils used in the laboratory tests that form the basis of the Olaya and Bray (2022b) postliquefaction volumetric strain model (e.g., soil fabric, time under sustained loading, OCR). Initially, the calibration factor was largely controlled by the Christchurch case histories because most of the natural soil deposit data are from Christchurch. To examine potential biases from the large set of Christchurch data, the residuals from a subset of non-Christchurch case histories, which lead to C = 1.36, were compared to the calibration factor of 1.71 obtained from the Christchurch case histories. The calibration factor was set to C = 1.50 to represent the conditions of a generic site. It is possible that the Christchurch case histories, with their robust LiDAR surveys, captured more ground settlement resulting from liquefaction than older case histories, or included ejecta-induced settlement not included in the older studies. The calibration factor is nearly one for hydraulic fills because the characteristics of hydraulic fills (i.e., relatively young, constructed soils with fabric similar that in the laboratory test programs) are better captured by the soils tested in the laboratory (i.e., C = 1.05 for hydraulic fill). The reason natural soils have C = 1.50 is not fully understood. It could be due in part to the systematically larger ground settlements measured in Christchurch through the LiDAR surveys, or it could be that the CPT liquefaction triggering and relative density correlations for natural soils are offset from those developed for constructed soil in the field and laboratory.

After C is applied to the results, residuals are plotted against I_{c15} , and the trends shown in Figs. 22(a and b) for hydraulic fills and natural soil deposits, respectively, can be eliminated by applying a soil behavior factor (SB) shown in Fig. 22(c) and calculated as

$$SB = \exp(-0.675 \cdot \max(I_{c_{15}}, 1.8) + 1.215)$$
 (12)

where I_{c15} = average I_c over a depth of 15 m as defined previously. A depth of 15 m was selected from statistical analyses of the depth that contributes significantly to settlement. The same SB value can be applied to the D_r -based and the ψ_o -based models without introducing significant biases.

Most of the bias in the residuals is eliminated with application of C and SB; however, a bias remained as a function of earthquake moment magnitude. Duration is captured in the calculation of FS_L through the magnitude scaling factor (MSF); thus, initially, another magnitude scaling factor was not thought to be required. However, the residuals indicated a dependence on M_w as shown in Figs. 23(a and b) for hydraulic fills and natural soil deposits, respectively. The observed trend in these residuals is eliminated by applying a magnitude factor (MF) as

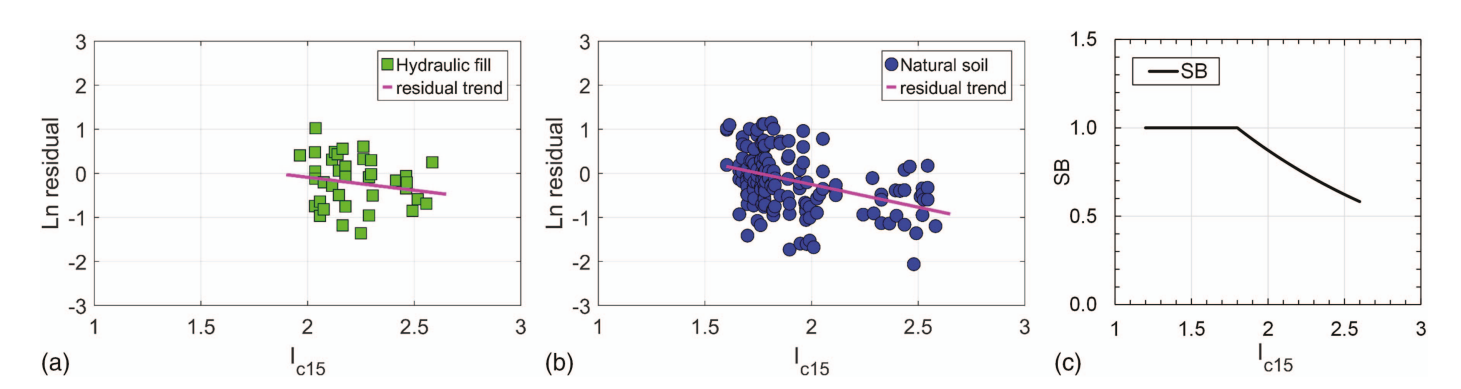


Fig. 22. (Color) Residuals $[\ln(S_{v_meas}) - \ln(S_{v_est})]$ versus I_{c15} for (a) hydraulic fill; (b) natural soil deposit; and (c) soil behavior factor relationship.

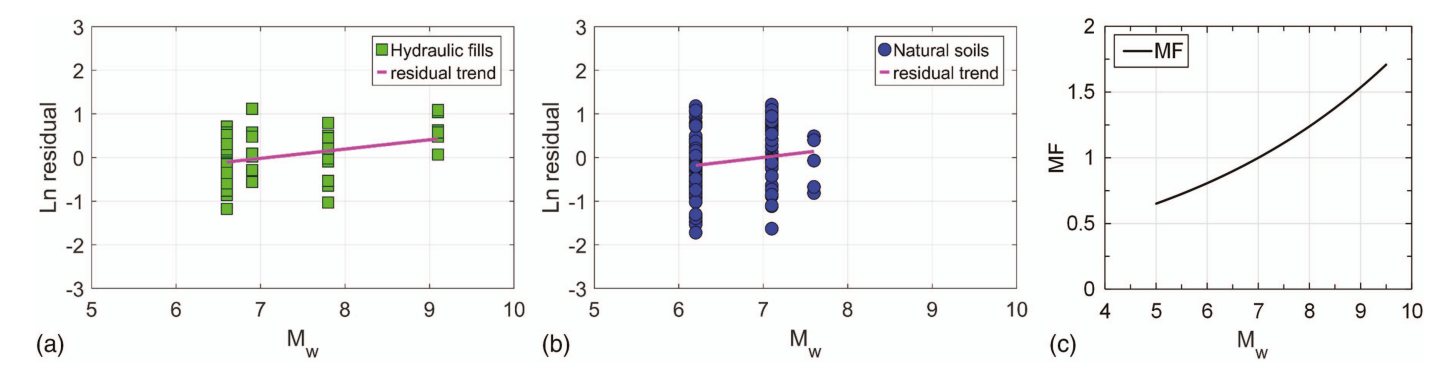


Fig. 23. (Color) Residuals $[\ln(S_{v_meas}) - \ln(S_{v_est})]$ versus M_w for (a) hydraulic fill; (b) natural soil deposit; and (c) magnitude factor relationship.

$$MF = \exp(0.214 \cdot M_w - 1.498) \tag{13}$$

The variation of MF with M_w is shown in Fig. 23(c). In retrospect, laboratory testing on sand specimens by Lee and Albaisa (1974) found that additional loading cycles applied beyond initial liquefaction induced larger volumetric strains, which indicates that larger M_w earthquakes with a larger number of equivalent cycles of loading should induce larger settlement, because liquefaction is typically triggered before the end of ground shaking in the case histories used to develop liquefaction-triggering procedures. The same MF value is applied to natural soil deposits and hydraulic fills using either the D_r -based or the ψ_o -based volumetric strain models.

Final Model

The final proposed model to estimate free-field postliquefaction ground settlement is

$$S_v = C \cdot MF \cdot SB \cdot \sum_{i} [\varepsilon_{vi} \cdot \Delta z_i] \cdot e^{\varepsilon}$$
 (14)

where the error term ε is normally distributed with zero mean and $\sigma=0.54$ in natural log units for hydraulic fill and $\sigma=0.61$ in natural log units for natural soil for the D_r -based volumetric strain model; and $\sigma=0.53$ and $\sigma=0.61$ for the hydraulic fill and natural soil, respectively, for the ψ_o -based volumetric strain model. As expected, the uncertainty is lower estimating postliquefaction ground settlement in constructed hydraulic fills than in natural soil deposits. Also, C=1.05 for hydraulic fills and C=1.50 for natural soil deposits for the reasons mentioned previously. Eq. (12) is used to calculate SB as a function of I_{c15} , and Eq. (13) is used to calculate MF as a function of M_w . As described previously, ε_{vi} is the postliquefaction volumetric strain calculated using the Olaya and Bray

(2022b) model, which is calculated using either its D_r -based or ψ_o -based $FS_{L-}\gamma_{\max}$ and $\gamma_{\max-}\varepsilon_v$ relationships, in which FS_L and D_r or ψ_o are estimated using CPT data at each depth i, and ΔZ_i is the thickness of the unit at depth i. The model is based on the mean estimate of FS_L with $P_L = 50\%$ using the two simplified liquefaction-triggering procedures mentioned previously and on the mean estimate of D_r or ψ_o using the two procedures mentioned previously.

The residuals for the final model for hydraulic fills and natural soil deposits are shown in Figs. 24(a and b), respectively. The final model provides reasonable estimates of liquefaction-induced ground settlement. The error term describes the uncertainty in the estimate of S_v given the values of the input parameters. In a deterministic assessment, the postliquefaction ground settlement should be provided as a likely range of settlement using the 16% and 84% values. In a probabilistic assessment, the uncertainty in the input parameters can be considered by including the uncertainty in the estimate of the ground motion parameter PGA in a seismic hazard assessment and by capturing the uncertainty in the key input parameters through a logic tree approach.

Illustrative Application of Procedure

The application of the proposed liquefaction-induced volumetric-induced ground-settlement procedure is illustrated using two case histories described in Olaya and Bray (2022a).

Case history CP-K16-S4 is a hydraulic fill site located in Wellington, New Zealand. The ground settlement is estimated for the 2016 Kaikoura M_w 7.8 earthquake that generated a nonliquefied site ground surface PGA = 0.25 g. The site has 10- to 20-m thick silty/sandy gravel fill atop marine sediments and alluvium that do not liquefy. The site is characterized by the six CPTs shown in Fig. 19, with the groundwater table located between 3.0–3.5 m

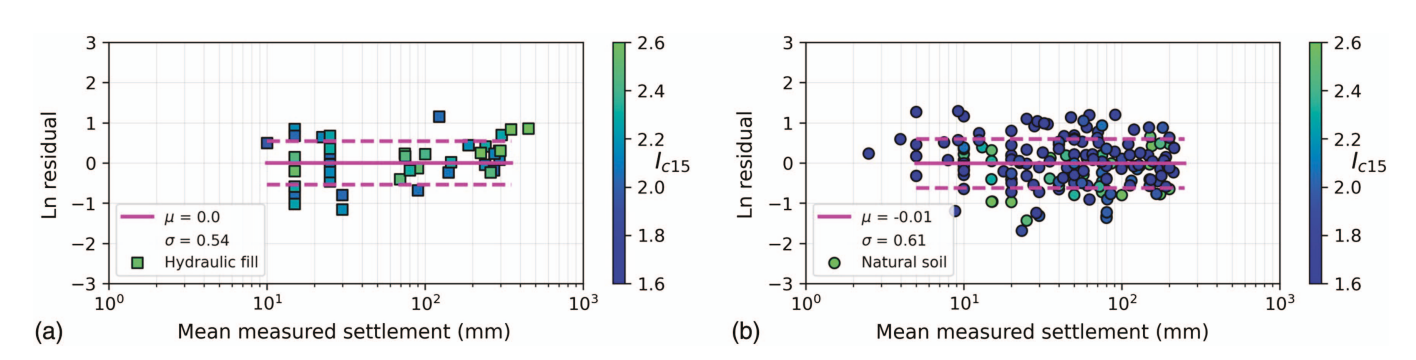


Fig. 24. (Color) Final model residuals $[\ln(S_{v_meas}) - \ln(S_{v_est})]$ for (a) hydraulic fill; and (b) natural soil deposit.

below the ground surface. I_{c15} varies between 1.91 and 2.25 for the six CPTs. The average of the D_r estimated using Eq. (8) and Robertson and Cabal (2015) varies between 30% and 95% in the profile; and the average of the $P_L = 50\% FS_L$ estimated using the Boulanger and Idriss (2016), Robertson and Wride (1998), Robertson (2009), and Ku et al. (2012) procedures varies between 0.30 and 2.0. Use of Eqs. (4) and (6) with the average D_r and FS_L values at each depth in the profile provides estimates of ε_v between 0% and 4.0%. SB is estimated to be between 0.74 and 0.93 using Eq. (12). MF is estimated as 1.19 using Eq. (13). C = 1.05 because it is a hydraulic fill. The median estimate of settlement for each of the six CPTs using Eq. (14) is between 225 and 425 mm with the site's geomean value of $S_v = 325$ mm and the 16% to 84% range of 190–550 mm ($\sigma = 0.54$). The estimated range of ground settlement is consistent with the surveyed ground settlement range of 200–350 mm (Dhakal et al. 2020).

Case history Ch-S167 is a natural soil deposit site located in Christchurch, New Zealand. Ground settlement is estimated for the 2011 M_w 6.2 June earthquake with a nonliquefied site ground surface PGA = 0.29 g. The site profile is composed primarily of silty sand layers with occasional lenses of clayey soil. The groundwater depth is estimated to be 2.0 m, and three CPTs are available at this site (Olaya and Bray 2022a). I_{c15} varies between 1.63 and 1.79. Following the same procedure as in the previous example, the average D_r varies between 20% and 90% in the profile, and the average of the $P_L = 50\% FS_L$ varies between 0.60 to 2.0. Use of Eqs. (4) and (6) with the average D_r and FS_L values at each depth provides estimates of ε_v between 0% and 3.6%. SB is estimated to be 1.0 $(I_{c15} < 1.8)$, MF = 0.84, and C = 1.50 (natural soil deposit). The median estimate of settlement for each of the three CPTs using Eq. (14) is between 50 and 80 mm, with the site's geomean value of $S_v = 60$ mm and the 16% to 84% range of 30–110 mm ($\sigma = 0.61$). The estimated range of ground settlement is consistent with the LiDAR-based measured settlement range of 30-90 mm (Olaya and Bray 2022a).

Liquefaction-Induced Building Settlement

Liquefaction-induced building settlement (S_t) is the combination of shear-induced settlement (S_s) , volumetric-induced settlement (S_v) , and ejecta-induced settlement (S_e) , as

$$S_t = S_s + S_v + S_e \tag{15}$$

Due to the related mechanisms of these liquefaction-induced building settlement components, the correlation among them should be considered. Currently, ejecta-induced settlement can be estimated using the approximate correlation of settlement with the general ejecta severity criteria of the CPT-based method proposed by Hutabarat and Bray (2022). There is insufficient statistical rigor to examine a correlation of S_e to S_v and S_s . Although uncertain, S_e is often negligible (e.g., at highly stratified soil sites). It is not often severe-to-extreme. In cases when it is minor or moderate, S_e is likely less than 50 mm or 100 mm, respectively. Mean best estimates of S_e are subtracted from S_t to analyze the joint occurrence of S_v and S_s for building-settlement case histories.

Bray and Macedo (2017) developed a set of 19 well documented liquefaction-induced building-settlement case histories with estimates of observed S_s , S_v , and S_e . These case histories are used to evaluate the relation between S_s and S_v after subtracting S_e , as explained above. The Bray and Macedo (2017) shear-based settlement model and the proposed volumetric-based model [Eq. (14)] are employed for the statistical evaluation of the correlation between S_s and S_v . These models are probabilistic and produce

normally distributed estimates of $ln(S_s)$ and $ln(S_v)$ with error terms that are zero-mean and normally distributed as

$$\ln(S_s) = f_s(\theta_s) + \delta_{S_s} \sigma_{S_s} \tag{16a}$$

$$\ln(S_v) = f_v(\theta_v) + \delta_{S_v} \sigma_{S_v}$$
(16b)

where $f_s(\theta_s)$ and $f_v(\theta_v)$ represent the parameters of each functional model; σ_{S_s} and σ_{S_v} are the models' standard deviations; and δ_{S_s} are the randomness in each model.

The correlation coefficient (ρ) between the residuals of the $\ln(S_s)$ and $\ln(S_v)$ models quantify the dependency between S_s and S_v (Baker and Cornell 2006). The relation between the residuals of the models for $\ln(S_s)$ and $\ln(S_v)$ using the available 19 case histories results in $\rho=0.72$. The correlation coefficient ρ is then employed to obtain correlated values of δ according to Eq. (17) (Baker and Cornell 2006), as

$$\delta_{S_v|S_s} = \rho \cdot \delta_{S_s} + N\sqrt{1 - \rho^2} \tag{17}$$

where N = normally distributed random variable with zero mean and unit standard deviation. Correlated samples for $\ln(S_s)$ and $\ln(S_v)$ can be generated by combining Eq. (17) with Eq. (16). A Monte Carlo approach with a sufficient number of realizations for $\ln(S_s)$ and $\ln(S_v)$ is then used to approximate the mean (μ_s) and standard deviation (σ_s) of $S_s + S_v$.

The application of the proposed liquefaction-induced buildingsettlement procedure is illustrated for the CTUC building site shown in Fig. 25 for the 2011 M_w 6.2 Christchurch earthquake. Observed settlements for the NE (Column A) and SE (Column F) corners of the building are provided in Luque and Bray (2017). No ejecta was observed near Column A, whereas S_e was estimated to be between 70 and 150 mm near Column F. Hence, the range of settlement after subtracting S_e is 160–260 mm near Column A and 250-450 mm near Column F of the building. At Column A, the Bray and Macedo (2017) median estimate of S_s is 70 mm with $\sigma_{S_c} = 0.50$ and the proposed model [Eq. (14)] median estimate of S_v is 100 mm with $\sigma_{S_v} = 0.61$. A set of 1,000 realizations of $S_s + S_v$ are produced using Eqs. (16) and (17), from which the estimated mean total settlement is 170 mm with a range of 100–290 mm ($\sigma_s = 0.53$ ln units). This settlement range is consistent with the observed settlement of 160-260 mm at Column A of the building. At Column F, the median estimate of S_s is 180 mm with $\sigma_{S_v} = 0.50$ and the median estimate of S_v is 140 mm with $\sigma_{S_v} = 0.61$. Again, a set of 1,000 realizations of $S_s + S_v$ are generated using Eqs. (16) and (17), from which the total median settlement is 325 mm with a range of 190–545 mm ($\sigma_s = 0.52$ ln units). This settlement range is also consistent with the observed settlement (without ejecta effects) of 250-450 mm at Column F of the building.

Conclusion

Great challenges remain in geotechnical earthquake engineering. Professor H. Bolton Seed forged a path that can be followed to advance knowledge in geotechnical earthquake engineering. Throughout his career, he integrated field case histories, laboratory experiments, and analyses in his studies. Analyses were not conducted to find the answer, but instead to gain insight. The authors employed Professor H. Bolton Seed's approach to evaluate liquefaction effects. Through examining field case histories, experiments, and analyses, insights are shared on the effects of liquefaction in the built environment.

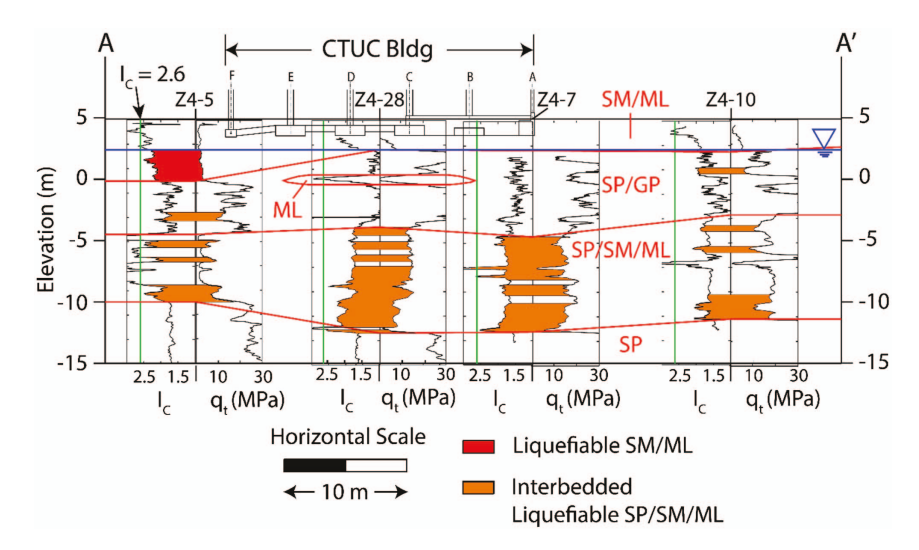


Fig. 25. (Color) CTUC building case history, Christchurch. (Reprinted from Luque and Bray 2017, © ASCE.)

Liquefaction-induced building settlement mechanisms are shear, volumetric, and ejecta. The problem is best viewed by examining soil response at the element level and soil deposit performance through its system response. The state of a unit of uniform clean sand, sandy gravel, nonplastic silty sand, and nonplastic silt can be examined in a unified manner using relative density and the state parameter. The cyclic responses of uniform fine sand, uniform nonplastic silty sand, and uniform coarse nonplastic silt are generally similar if at the same state and effective confining stress and loaded similarly. Postliquefaction volumetric strain models are presented that capture this important soil response in a unified manner. In many cases, sandy gravels that are controlled by their sand matrix and clayey silts that respond similarly to nonplastic silts can be captured using models developed for sand, silty sand, and nonplastic silt.

The system response of a soil deposit often governs the consequences of liquefaction triggering. System response features greatly affect the formation of ejecta and its effects on infrastructure. Ejecta-induced building settlement is challenging to estimate. However, through dynamic nonlinear effective stress analysis, the importance of capturing the postshaking hydraulic mechanisms that govern the upward flow of water was identified. The ejecta potential index indicates when ejecta is likely to occur and how extensive it would likely be when it occurs. A CPT-based method can be used to evaluate ejecta severity when there are insufficient resources to support effective stress analyses. Its liquefaction ejecta demand parameter L_D tends to increase systematically as ejecta severity increases at thick clean sand sites. Low L_D values are estimated at stratified soil sites that did not produce ejecta, which resolves the apparent overestimation by other liquefaction indices at stratified soil sites. The $L_D - C_R$ liquefaction ejecta severity chart separates cases with severe or extreme ejecta, which have high L_D and low C_R values, from cases with no ejecta, which have low L_D and high C_R values. The CPT-based liquefaction ejecta severity chart provides a preliminary estimate of the free-field, level-ground, ejectainduced ground settlement using Table 2.

The CPT should be the primary site investigation tool in most liquefaction evaluations. The CPT should be complemented with cyclic tests performed on high-quality samples when they are informative. The insights derived from cyclic tests support effective stress analyses, which provide additional insights. However, there is no substitute for characterizing the depositional environment. Geologic details matter. Soil fabric is only indirectly assessed through most field and laboratory testing methods. Detailed logging

of high-quality continuous samples to examine soil fabric and other important details should be performed when it is suspected that key factors will be missed using conventional sampling and in situ testing.

A probabilistic CPT-based postliquefaction ground-settlement procedure is proposed. It takes advantage of a recently compiled comprehensive laboratory database of postliquefaction testing and a recently compiled comprehensive database of field case histories of postliquefaction settlement measurements. The volumetric strain of nonplastic soil with uniform gradation (SP, SM, and ML) can be estimated using D_r -based or ψ_o -based volumetric strain models. New correlations are developed to estimate D_r or ψ_o to enable use of the volumetric strain models. A calibration factor is required to adjust the estimates of natural soil deposits, as these deposits have characteristics that are not well represented in the laboratory tests used to develop the volumetric strain models. The calibration factor is nearly one for hydraulic fills. A soil behavior factor dependent on I_{c15} and a magnitude factor dependent on M_w are incorporated in the model to capture their effects on postliquefaction ground settlement. The calibrated model captures the trends in the field measurements of postliquefaction ground settlement well.

Additional studies to develop alternative models and perspectives are warranted. As stated previously, great challenges remain in geotechnical earthquake engineering, especially in the evaluation of liquefaction effects. Liquefaction research can advance the state-of-the-art by focusing on understanding and evaluating the effects of liquefaction and developing innovative mitigation methodologies.

Data Availability Statement

Some or all data, models, or code that support the findings of this study are available from the corresponding author upon reasonable request.

Acknowledgments

Support for this research was provided primarily by grants from the US National Science Foundation (NSF) through CMMI-1956248 and the California Department of Transportation (Caltrans) through Agreement 65A0774 Amendment TO-005. The findings, opinions, and conclusions presented in this paper are those of the authors and

do not necessarily reflect the views of the sponsors. The NSFsponsored Geotechnical Extreme Events Reconnaissance (GEER) Association funding through Grant CMMI-1266418 enabled researchers to document and learn from the case histories discussed in this article. Additionally, the College of Engineering at the University of California, Berkeley (UCB), provided support through the Faculty Chair in Earthquake Engineering Excellence. The numerous significant contributions of Professor H. Bolton Seed over his distinguished career are recognized. Prof. Kenji Ishihara also provided data, insights, and inspiration for this work. Zorana Mijic and Daniel Hutabarat of UCB shared data and insights from their Ph.D. research. We acknowledge the efforts of all GEER team members who participated in postearthquake reconnaissance relied upon in this study. We thank Misko Cubrinovski of the University of Canterbury, who shared data and concepts freely, and those whose research supported this study, including Michael Riemer, Rodolfo Sancio, Jennifer Donahue, Christine Beyzaei, Christopher Markham, Claudio Cappellaro, Sean Rees, Ribu Dhakal, Jorge Macedo, Roberto Luque, Josh Zupan, Mark Stringer, Merrick Taylor, Tom O'Rourke, Brendon Bradley, Sjoerd Van Ballegooy, Mike Jacka, Rick Wentz, Ian McCahon, Nick Traylen, and Iain Haycock. We also thank Uri Eliahu and Pedro Espinosa of ENGEO, Inc., for providing CPT data for Treasure Island, the team of engineers who worked on the Treasure Island project, which included P. Espinosa, P. Stuecheli, S. Papadopoulos, J. Tootle, U. Eliahu, S. Vahdani, B. Heidarzadeh, S. Dickenson, M. Beaty, J. Pestana, N. Sitar, M. Riemer, and C. Markham. R. Luna and J. P. Bardet provided CPT data for Treasure Island and the Marina District, respectively. The New Generation Liquefaction project provided access to data. Norman Abrahamson of UCB assisted in the development of the probabilistic models. Ross Boulanger of UC Davis provided useful feedback after the Seed Lecture.

References

- Akai, K., et al. 1995. Geotechnical reconnaissance of the effects of the January 17, 1995, Hyogoken-Nanbu Earthquake, Japan. Earthquake Engineering Research Center Rep. No. UCB/EERC-95/01. Berkeley, CA: Univ. of California, Berkeley.
- Baker, J. W., and C. A. Cornell. 2006. "Correlation of response spectral values for multi-component ground motions." *Bull. Seismol. Soc. Am.* 96 (1): 215–227. https://doi.org/10.1785/0120050060.
- Been, K., and M. G. Jefferies. 1985. "A state parameter for sands." *Géotechnique* 35 (2): 99–112. https://doi.org/10.1680/geot.1985.35.2.99.
- Beyzaei, C. Z. 2017. "Fine-grained soil liquefaction effects in Christchurch, New Zealand." Ph.D. thesis, Dept. of Civil and Environmental Engineering, Univ. of California, Berkeley.
- Beyzaei, C. Z., J. D. Bray, M. Cubrinovski, M. Riemer, and M. Stringer. 2018a. "Laboratory-based characterization of shallow silty soils in southwest Christchurch." Soil Dyn. Earthquake Eng. 110 (Jul): 93–109. https:// doi.org/10.1016/j.soildyn.2018.01.046.
- Beyzaei, C. Z., J. D. Bray, S. Cubrinovski, S. Bastin, M. Riemer, M. Stringer, M. Jacka, S. van Ballegooy, and R. Wentz. 2020. "Characterization of silty soil thin-layering and groundwater conditions for liquefaction assessment." Can. Geotech. J. 57 (2): 263–276. https://doi.org/10.1139/cgj -2018-0287.
- Beyzaei, C. Z., J. D. Bray, S. van Ballegooy, S. Cubrinovski, and S. Bastin. 2018b. "Depositional environment effects on observed liquefaction performance in silt swamps during the Canterbury earthquake sequence." Soil Dyn. Earthquake Eng. 107 (Apr): 303–321. https://doi.org/10.1016 /j.soildyn.2018.01.035.
- Bolton, M. D. 1986. "The strength and dilatancy of sands." *Géotechnique* 36 (1): 65–78. https://doi.org/10.1680/geot.1986.36.1.65.
- Boulanger, R. W., and I. M. Idriss. 2008. "Closure to 'Evaluation of cyclic softening in silts and clays' by Ross W. Boulanger and I. M. Idriss."

- J. Geotech. Geoenviron. Eng. 135 (2): 308. https://doi.org/10.1061/(ASCE)1090-0241(2009)135:2(308).
- Boulanger, R. W., and I. M. Idriss. 2016. "CPT-based liquefaction triggering procedures." J. Geotech. Geoenviron. Eng. 142 (2): 04015065. https://doi. org/10.1061/(ASCE)GT.1943-5606.0001388.
- Bray, J. D., et al. 2004. "Subsurface characterization at ground failure sites in Adapazari, Turkey." *J. Geotech. Geoenviron. Eng.* 130 (7): 673–685. https://doi.org/10.1061/(ASCE)1090-0241(2004)130:7(673).
- Bray, J. D., R. W. Boulanger, M. Cubrinovski, K. Tokimatsu, S. L. Kramer, T. O'Rourke, E. Rathje, R. A. Green, P. Robertson, and C. S. Beyzaei. 2017. US–New Zealand–Japan international workshop, liquefaction-induced ground movements effects. PEER Rep. No. 2. Berkeley, CA: Univ. of California, Berkeley.
- Bray, J. D., M. Cubrinovski, J. Zupan, and M. Taylor. 2014a. "CPT-based liquefaction assessments in Christchurch, New Zealand." In *Proc.*, CPT'14: 3rd Int. Symp. on Cone Penetration Testing. Las Vegas: Omnipress US.
- Bray, J. D., M. Cubrinovski, J. Zupan, and M. Taylor. 2014b. "Liquefaction effects on buildings in the central business district of Christchurch." *Earthquake Spectra* 30 (1): 85–109. https://doi.org/10.1193/022113 EQS043M.
- Bray, J. D., and J. Macedo. 2017. "6th Ishihara lecture: Simplified procedure for estimating liquefaction-induced building settlement." Soil Dyn. Earthquake Eng. 102 (Nov): 215–231. https://doi.org/10.1016/j.soildyn.2017.08.026.
- Bray, J. D., and R. B. Sancio. 2006. "Assessment of the liquefaction susceptibility of fine-grained soils." *J. Geotech. Geoenviron. Eng.* 132 (9): 1165–1177. https://doi.org/10.1061/(ASCE)1090-0241(2006)132:9 (1165).
- Bray, J. D., and R. B. Sancio. 2008. "Closure to 'Assessment of the lique-faction susceptibility of fine-grained soils' by Jonathan D. Bray and Rodolfo B. Sancio." *J. Geotech. Geoenviron. Eng.* 134 (7): 1031–1034. https://doi.org/10.1061/(ASCE)1090-0241(2008)134:7(1031).
- Bray, J. D., and J. P. Stewart. 2000. "Damage patterns and foundation performance in Adapazari." *Earthquake Spectra J.* 1 (Suppl A): 163–189. https://doi.org/10.1193/1.1586152.
- Bullock, Z., Z. Karimi, S. Dashti, K. Porter, A. B. Liel, and W. Franke. 2019. "A physics-informed semi-empirical probabilistic model for the settlement of shallow-founded structures on liquefiable ground." Géotechnique 69 (5): 406–419. https://doi.org/10.1680/jgeot.17.P.174.
- Cetin, K. O., H. T. Bilge, J. Wu, A. M. Kammerer, and R. B. Seed. 2009. "Probabilistic model for the assessment of cyclically induced reconsolidation (volumetric) settlements." *J. Geotech. Geoenviron. Eng.* 135 (3): 387–398. https://doi.org/10.1061/(ASCE)1090-0241(2009)135:3(387).
- Cubrinovski, M. 2019. "Some important considerations in the engineering assessment of soil liquefaction." In *Proc., 13th Australia New Zealand Conf. on Geomechanics*, 19–36. Sydney, Australia: Australian Geomechanics Society.
- Cubrinovski, M., J. D. Bray, C. de la Torre, M. Olsen, B. A. Bradley, G. Chiaro, E. Stocks, L. Wotherspoon, and T. Krall. 2018a. "Liquefactioninduced damage and CPT characterization of the reclamations at Centre-Port, Wellington." *Bull. Seismol. Soc. Am.* 108 (3B): 1695–1708. https:// doi.org/10.1785/0120170246.
- Cubrinovski, M., J. D. Bray, M. Taylor, S. Giorgini, B. Bradley, L. Wotherspoon, and J. Zupan. 2011. "Soil liquefaction effects in the central business district during the February 2011 Christchurch earthquake." Seismol. Res. Lett. 82 (6): 893–904. https://doi.org/10 .1785/gssrl.82.6.893.
- Cubrinovski, M., and K. Ishihara. 2002. "Maximum and minimum void ratio characteristics of sands." *Soils Found.* 42 (6): 65–78. https://doi.org/10.3208/sandf.42.6_65.
- Cubrinovski, M., A. Rhodes, N. Ntritsos, and S. van Ballegooy. 2018b. "System response of liquefiable deposits." *Soil Dyn. Earthquake Eng.* 124 (Sep): 212–229. https://doi.org/10.1016/j.soildyn.2018.05.013.
- Dhakal, R., M. Cubrinovski, and J. D. Bray. 2020. "Geotechnical characterization and liquefaction evaluation of gravelly reclamations and hydraulic fills (Port of Wellington, New Zealand)." Soils Found. 60 (6): 1507–1531. https://doi.org/10.1016/j.sandf.2020.10.001.
- Dhakal, R., M. Cubrinovski, and J. D. Bray. 2022. "Evaluating the applicability of conventional CPT-based liquefaction assessment procedures

- to reclaimed gravelly soils." *Soil Dyn. Earthquake Eng.* 155 (Apr): 107176. https://doi.org/10.1016/j.soildyn.2022.107176.
- Dobry, R., and R. Ladd. 1980. "Discussion on 'Soil liquefaction and cyclic mobility evaluation for level ground during earthquakes and liquefaction potential: Science versus practice." *J. Geotech. Eng. Div.* 106 (6): 720–724. https://doi.org/10.1061/AJGEB6.0000984.
- Donahue, J. L., J. D. Bray, and M. F. Riemer. 2007. "Liquefaction testing of fine-grained soil prepared using slurry deposition." In *Proc.*, 4th Int. Conf. Earthquake Geotechnical Engineering. Berlin: Springer.
- Dooku, P. M., P. M. Stewart, D. H. Whang, and E. Yee. 2008. "Volumetric strains of clean sands subject to cyclic loads." *J. Geotech. Eng. Div.* 134 (8): 1073–1085. https://doi.org/10.1061/(ASCE)1090-0241(2008) 134:8(1073).
- Duncan, J. M., S. G. Wright, and T. L. Brandon. 2014. Soil strength and slope stability. New York: Wiley.
- ENGEO. 2016. Dynamic behavior of the treasure Island natural shoal deposit. Rep. No. 7091.000.000-T4. San Francisco: ENGEO.
- Hutabarat, D., and J. D. Bray. 2021a. "Effective stress analysis of liquefiable sites to estimate the severity of sediment ejecta." J. Geotech. Eng. Div. 147 (5): 04021040. https://doi.org/10.1061/(ASCE)GT.1943-5606.0002506.
- Hutabarat, D., and J. D. Bray. 2021b. "Seismic response characteristics of liquefiable sites with and without sediment ejecta manifestation." J. Geotech. Eng. Div. 147 (6): 04021040. https://doi.org/10.1061/(ASCE)GT .1943-5606.0002506.
- Hutabarat, D., and J. D. Bray. 2022. "Estimating the severity of liquefaction ejecta using the cone penetration test." J. Geotech. Eng. Div. 148 (3): 04021195. https://doi.org/10.1061/(ASCE)GT.1943-5606.0002744.
- Idriss, I., and R. Boulanger. 2008. Soil liquefaction during earthquakes. Oakland, CA: Earthquake Engineering Research Institute.
- Ishihara, K. 1993. "Liquefaction and flow failure during earthquakes." Géotechnique 43 (3): 351–451. https://doi.org/10.1680/geot.1993.43 .3.351.
- Ishihara, K., and M. Yoshimine. 1992. "Evaluation of settlements in sand deposits following liquefaction during earthquakes." Soils Found. 32 (1): 173–188. https://doi.org/10.3208/sandf1972.32.173.
- Iwasaki, T., F. Tatsuoka, K. Tokida, and S. Yasuda. 1978. "A practical method for assessing soil liquefaction potential based on case studies at various sites in Japan." In *Proc.*, 2nd Int. Earthquake Microzonation Conf., 885–896. Washington, DC: National Science Foundation.
- Jefferies, M., and K. Been. 2016. *Soil liquefaction: A critical state approach*. 2nd ed. Boca Raton, FL: Taylor & Francis Group.
- JGS (Japanese Geotechnical Society). 2000. Test methods for minimum and maximum densities of sands. JIS A 1224:2000. Tokyo: JGS.
- Ku, C. S., C. H. Juang, C. W. Chang, and J. Ching. 2012. "Probabilistic version of the Robertson and Wride method for liquefaction evaluation: Development and application." *Can. Geotech. J.* 49 (1): 27–44. https://doi.org/10.1139/t11-085.
- Ladd, R. S. 1977. "Specimen preparation and cyclic stability of sands." J. Geotech. Eng. Div. 103 (6): 535–547. https://doi.org/10.1061 /AJGEB6.0000435.
- Lee, K. L., and A. Albaisa. 1974. "Earthquake induced settlements in saturated sands." J. Geotech. Eng. Div. 100 (4): 387–406. https://doi.org/10.1061/AJGEB6.0000034.
- Luque, R., and J. D. Bray. 2017. "Dynamic analyses of two buildings founded on liquefiable soils during the Canterbury earthquake sequence." J. Geotech. Geoenviron. Eng. 143 (9): 04017067. https://doi .org/10.1061/(ASCE)GT.1943-5606.0001736.
- Markham, C. S. 2015. "Response of liquefiable sites in the central business district of Christchurch, New Zealand." Ph.D. thesis, Dept. of Civil and Environmental Engineering, Univ. of California, Berkeley.
- Markham, C. S., J. D. Bray, M. Cubrinovski, and M. Riemer. 2018. "Lique-faction resistance and steady-state characterization of shallow soils within the Christchurch Central Business District." J. Geotech. Geoenviron. Eng. 144 (6): 04018032. https://doi.org/10.1061/(ASCE)GT.1943-5606.0001823.
- Markham, C. S., J. D. Bray, M. F. Riemer, and M. Cubrinovski. 2016. "Characterization of shallow soils in the central business district of Christchurch, New Zealand." *Geotech. Test. J.* 39 (6): 922–937. https://doi.org/10.1520/GTJ2015024.

- Mayne, P. W., and M. Styler. 2018. "Soil liquefaction screening using CPT yield stress profiles." In Proc., Geotechnical Earthquake Engineering and Soil Dynamics V: Liquefaction Triggering, Consequences, and Mitigation, 605–616. Reston, VA: ASCE.
- Mijic, Z., J. D. Bray, M. F. Riemer, M. Cubrinovski, and S. D. Rees. 2021a. "Test method for minimum and maximum densities of small quantities of soil." *Soils Found*. 61 (2): 533–540. https://doi.org/10.1016/j.sandf.2020.12.003.
- Mijic, Z., J. D. Bray, M. F. Riemer, S. D. Rees, and M. Cubrinovski. 2021b. "Cyclic and monotonic simple shear testing of native Christchurch silty soil." *Soil Dyn. Earthquake Eng.* 148 (Sep): 106834. https://doi.org/10 .1016/j.soildyn.2021.106834.
- Mijic, Z., J. D. Bray, and S. van Ballegooy. 2022. "Liquefaction ejecta case histories for 2010–11 Canterbury earthquakes." *Int. J. Geo-Eng. Case Hist.* 6 (3): 73–93. https://doi.org/10.4417/IJGCH-06-03-04.
- Mitchell, J., and K. Soga. 2005. Fundamentals of soil behavior. 3rd ed. New York: Wiley.
- Mulilis, J. P., H. B. Seed, C. K. Chan, J. K. Mitchell, and K. Arulanandan. 1977. "Effects of sample preparation on sand liquefaction." *J. Geotech. Eng. Div.* 103 (2): 91–108. https://doi.org/10.1061/AJGEB6.0000387.
- Olaya, F. R., and J. D. Bray. 2022a. CPT case histories of post-liquefaction free-field ground settlement. Geosystems Engineering Rep. No. UCB/GT 2022-02. Berkeley, CA: Univ. of California, Berkeley.
- Olaya, F. R., and J. D. Bray. 2022b. "Strain potential of liquefied soil." J. Geotech. Geoenviron. Eng. 148 (11): 04022099. https://doi.org/10.1061/(ASCE)GT.1943-5606.0002896.
- Polito, C. P., and J. R. Martin II. 2001. "Effects of nonplastic fines on the liquefaction resistance of sands." J. Geotech. Geoenviron. Eng. 127 (5): 408–415. https://doi.org/10.1061/(ASCE)1090-0241(2001)127:5(408).
- Robertson, P. K. 2009. "Performance-based earthquake design using the CPT." In Proc., Int. Conf. on Performance—Based Design in Earthquake Geotechnical Engineering. Tokyo: Taylor & Francis.
- Robertson, P. K. 2010. "Estimating in-situ state parameter and friction angle in sandy soils from CPT." In *Proc.*, 2nd Int. Symp. on Cone Penetration Testing. Signal Hill, CA: Gregg Drilling & Testing.
- Robertson, P. K. 2016. "Cone penetration test (CPT)-based soil behaviour type (SBT) classification system—An update." Can. Geotech. J. 53 (12): 1910–1927.
- Robertson, P. K., and K. L. Cabal. 2015. *Guide to CPT for geotechnical engineering*. 6th ed. Signal Hill, CA: Gregg Drilling Testing.
- Robertson, P. K., and C. E. Wride. 1998. "Evaluating cyclic liquefaction potential using the cone penetration test." *Can. Geotech. J.* 35 (3): 442–459. https://doi.org/10.1139/t98-017.
- Russell, J., and S. van Ballegooy. 2015. Canterbury earthquake sequence: Increased liquefaction vulnerability assessment methodology. T+T Rep. No. 0028-1-R-JICR-2015. Earthquake Commission. Auckland, New Zealand: Tonkin & Taylor.
- Seed, H. B. 1979. "Soil liquefaction and cyclic mobility evaluation for level ground during earthquakes." J. Geotech. Eng. Div. 105 (2): 201–255. https://doi.org/10.1061/AJGEB6.0000768.
- Shamoto, Y., M. Sato, and J. Zhang. 1996. "Simplified estimation of earthquake-induced settlements in saturated sand deposits." *Soils Found.* 36 (1): 39–50. https://doi.org/10.3208/sandf.36.39.
- Shuttle, D. A., and J. Cunning. 2007. "Liquefaction potential of silts from CPTu." *Can. Geotech. J.* 45 (1): 140–141. https://doi.org/10.1139/t06-086.
- Shuttle, D. A., and J. Cunning. 2008. "Reply to the discussion by Robertson on liquefaction potential of silts from CPTu." *Can. Geotech. J.* 45 (1): 142–145. https://doi.org/10.1139/T07-119.
- Tatsuoka, F., S. Zhou, T. Sato, and S. Shibuya. 1990. "Method of evaluating liquefaction potential and its application." [In Japanese.] In *Report on seismic hazards on the ground in urban areas*. Tokyo: Ministry of Education of Japan.
- Thevanayagam, S., T. Shenthan, S. Mohan, and J. Liang. 2002. "Undrained fragility of clean sands, silty sands, and sandy silts." *J. Geotech. Geoenviron. Eng.* 128 (10): 849–859. https://doi.org/10.1061/(ASCE)1090-0241(2002)128:10(849).
- Toriihara, M., Y. Yamada, I. Morimoto, and K. Ishihara. 2000. "The characteristics of settlement after liquefaction for sand containing fines."

- [In Japanese.] In Vol. 3 of *Proc.*, 35th Japan Conf. on Geotechnical Engineering, 1655–1656. Tokyo: Japanese Geotechnical Society.
- van Ballegooy, S., P. Malan, V. Lacrosse, M. E. Jacka, M. Cubrinovski, J. D. Bray, T. D. O'Rourke, S. A. Crawford, and H. Cowan. 2014. "Assessment of liquefaction-induced land damage for residential christ-church." *Earthquake Spectra J.* 30 (1): 31–55. https://doi.org/10.1193/031813EQS070M.
- Whang, D. H. 2001. "Seismic compression of compacted soils." Ph.D. thesis, Dept. of Civil and Environmental Engineering, Univ. of California.
- Yasuda, S., K. Ishihara, K. Harada, and N. Shinkawa. 1996. "Effect of soil improvement on ground subsidence due to liquefaction." Soils Found. 36 (Jun): 99–107. https://doi.org/10.3208/sandf.36.Special_99.
- Yoshimine, M., H. Nishizaki, K. Amano, and Y. Hosono. 2006. "Flow deformation of liquefied sand under constant shear load and its

- applications to analysis of flow slide in infinite slope." *Soil Dyn. Earthquake Eng.* 26 (2–4): 253–264. https://doi.org/10.1016/j.soildyn.2005.02.016.
- Youd, T., and D. Perkins. 1978. "Mapping liquefaction-induced ground failure potential." J. Geotech. Eng. Div. 104 (4): 433–446. https://doi.org/10.1061/AJGEB6.0000612.
- Zhang, G., P. K. Robertson, and R. W. I. Brachman. 2002. "Estimating liquefaction-induced ground settlements from CPT for level ground." Can. Geotech. J. 39 (5): 1168–1180. https://doi.org/10.1139/t02-047.
- Zhang, G., P. K. Robertson, and R. W. I. Brachman. 2004. "Estimating liquefaction induced lateral deformations from SPT and CPT." J. Geotech. Geoenviron. Eng. 130 (8): 861–871. https://doi.org/10.1061/(ASCE)1090-0241(2004)130:8(861).